

Coherence and de-coherence in the Time-Resolved ARPES of realistic materials: an ab-initio perspective

Andrea Marini

Istituto di Struttura della Materia and Division of Ultrafast Processes in Materials (FLASHit) of the National Research Council, via Salaria Km 29.3, I-00016 Monterotondo Stazione, Italy

European Theoretical Spectroscopy Facilities (ETSF)

Enrico Perfetto

Dipartimento di Fisica, Università di Roma Tor Vergata, Via della Ricerca Scientifica 1, 00133 Rome, Italy

Gianluca Stefanucci

Dipartimento di Fisica, Università di Roma Tor Vergata, Via della Ricerca Scientifica 1, 00133 Rome, Italy

Abstract

Coherence and de-coherence are the most fundamental steps that follow the initial photo-excitation occurring in typical P&p experiments. Indeed, the initial external laser pulse transfers coherence to the system in terms of creation of multiple electron-hole pairs excitation. The excitation concurs both to the creation of a finite carriers density and to the appearance of induced electromagnetic fields. The two effects, to a very first approximation, can be connected to the simple concepts of populations and oscillations. The dynamics of the system following the initial photo-excitation is, thus, entirely dictated by the interplay between coherence and de-coherence. This interplay and the de-coherence process itself, is due to the correlation effects stimulated by the photo-excitation. Single-particle, like the electron-phonon, and two-particles, like the electron-electron, scattering processes induce a complex dynamics of the electrons that, in turn, makes the description of the correlated and photo-excited system in terms of pure excitonic and/or carriers populations challenging.

Contents

1 Introduction

3

2	Motivations	4
2.1	Photo-induced coherence: preliminary remarks	5
2.2	The paradigmatic case of the carrier lifetimes. Are they really intrinsic quantities?	7
3	Interacting electrons: Hamiltonian and potentials	9
3.1	The reference ab-initio system	11
3.2	A model Hamiltonian	12
4	Ab-Initio Many-Body Perturbation Theory	13
4.1	Quasiparticles and lifetimes	16
4.1.1	Specific Self-Energy approximations	18
4.2	Neutral excitation: plasmons and excitons	22
4.2.1	Potentials and response functions	22
4.2.2	The Bethe-Salpeter equation(s)	24
5	Ab-Initio Non-Equilibrium Green's Function Theory	25
5.1	NEGF and connection to observable quantities	26
5.2	From the full Kadanoff-Baym equations to the single-time evolution method	27
5.3	The Markovian approximation	30
5.4	Equilibrium self-energies taken out-of-equilibrium	31
6	Time-Resolved ARPES	32
6.1	Coherent and incoherent regimes: preliminary remarks	34
6.1.1	Excitonic signatures in the coherent regime of the model system	36
6.2	Incoherent regime: excitons versus quasiparticles	42
6.2.1	Incoherent excitonic contribution in the model system	43
6.2.2	Coherent excitation and incoherent carriers migration	47
6.3	Time-Resolved ARPES from first-principles in two paradigmatic materials: bulk Silicon and Black-Phosphorus	51
6.3.1	Symmetry breaking and ultra-fast restoring in Bulk Silicon	51

6.3.2	Photocarrier-induced band-gap renormalization and ultrafast charge dynamics in black phosphorus	54
7	Conclusion and perspectives	56
8	Acknowledgments	57

1. Introduction

Time-resolved (TR) and angle-resolved photo-emission spectroscopy (ARPES) has established as a powerful experimental technique to monitor the ultrafast dynamics of electronic excitation in materials. Applications cover image potential states [1, 2, 3, 4, 5, 6] electron relaxation in metals [7, 8, 9, 10] semiconductors [11, 12, 13, 14] and more recently topological insulators [15, 16, 17, 18, 19, 20], charge transfer processes at solid state interfaces [21, 22, 23, 24, 25] and in adsorbate on surfaces [26, 27, 28, 29, 30, 31, 32] and the formation and dynamics of excitons [11, 12, 33, 34, 35, 36].

In TR-ARPES on semiconductors or insulators a coherent laser pulse excites electrons from the valence band to the conduction band. During pumping and for about a few hundreds of femtoseconds after several semiconductors with a gap of 1 eV or larger [37, 38, 39, 40] coherently oscillate between the ground state and the dipole-allowed excited states. Due to the Coulomb attraction between the conduction electrons and the valence holes the excited states may also contain bound electron-hole (*eh*) pairs or *excitons*. These excitons are said *coherent* or *virtual* [41, 42, 43] since they give rise to an oscillating (in time) polarization of the medium. After tens of picoseconds coherence is destroyed by electron-electron [44, 45] and electron-phonon [46, 47] scattering processes. The system reaches a quasi-equilibrium state characterized by quasi-free carriers coexisting with *incoherent* or real excitons [48, 49, 50]. In this steady regime the electronic density matrix is not a pure state but an admixture of the ground state and dressed electron-hole excited states.

The photocurrent of a TR-ARPES experiment is generated by a *probe* pulse impinging the system. The spectrum depends on the intensity and frequency of the pump excitation, on the delay between pump and probe as well as on the duration of the

probe [51]. Therefore TR-ARPES provides a unique tool to reveal different excitation and in particular to characterize the nature of what is generally defined an “exciton”. In fact, excitonic structures inside the gap can change their shape, position and intensity, meaning that excited states with different excitonic character are visited.

In this work we will first give, in Section 2, some motivations to the device of a microscopic theory of Many-Body systems at and out-of equilibrium. We will discuss how a P&p experiment can actually trigger phenomena specific to the excitation process and also induce the coherent formation of high energy states. We will then introduce, in Section 3 the main mathematical ingredients of the Hamiltonian considered in this work. Two different reference systems will be used: a fully *ab-initio* scheme based on Density-Functional Theory, Section 3.1, and a two-bands model Hamiltonian, Section 3.2, that will allow to highlight some key aspects in a transparent way.

After reviewing, in Section 4 the equilibrium Many-Body theory in order to introduce key concepts like quasiparticles and excitons, we will move out-of-equilibrium in Section 5. The different self-energies used both at equilibrium and out-of-equilibrium are introduced in Section 4.1.1.

The third part of this work is entirely devoted to the TR-ARPES. We will first introduce the concepts of coherent and in-coherent regime in Section 6.1. We will then use two very different approaches in the two regimes. We will first investigate coherent excitonic effects by using a simple model Hamiltonian in Section 6.1.1. The same Hamiltonian will be used in Section 6.2.1 to describe the very different nature of bound electron-hole pairs in the in-coherent regime, i.e. after the induced polarization has died.

We will end this section with the *ab-initio* approach to TR-ARPES. The *ab-initio* NEGF approach will be first reviewed in Section 6.2.2 and later applied to two paradigmatic materials: bulk Silicon (Section 6.3.1) and Black-Phosphorus (Section 6.3.2).

2. Motivations

It would be very much desirable to be able to interpret the photo-excited materials in terms of simple arguments, taken from the equilibrium physics. This, indeed, is

often based on simple concepts that can make the interpretation of the complex real-time dynamics appealing. As a matter of fact, instead, the photo-excitation takes the system in an highly intricated state that, even by using advanced Many-Body concepts, is difficult to describe accurately.

This motivates a careful and deep investigation of the physics out-of-equilibrium especially when applied to realistic materials. In order to motivate this, by using simple arguments, in the next two sections we will investigate two paradigmatic properties of a photo-excited material: the connection between photo-excitation and coherence and the actual modification of the microscopic, elemental, scattering processes induced by the experimental pump field.

2.1. Photo-induced coherence: preliminary remarks

To interpret ARPES spectra of photoexcited materials it is crucial to have a proper description of the nonequilibrium state of the system. Depending on the delay between the pump and probe pulses the nonequilibrium state of interest could be the one describing the system subject to an electromagnetic perturbation (overlapping pump and probe), or shortly after the pump (coherent regime) or after the complete loss of coherence (incoherent regime). The differences between these different regimes can already be highlighted using a simple two-level system, the lowest (highest) level representing the valence (conduction) band, coupled through a dipole moment D to an electric field $E(t)$:

$$\hat{H}(t) = \hat{h}_e + \hat{V}_{e-\gamma}(t), \quad (1a)$$

$$\hat{h}_e = \sum_{i=c,v} \epsilon_i \hat{d}_i^\dagger \hat{d}_i, \quad (1b)$$

$$\hat{V}_{e-\gamma}(t) = E(t) \left(D \hat{d}_c^\dagger \hat{d}_v + D^* \hat{d}_v^\dagger \hat{d}_c \right). \quad (1c)$$

Letting $|\Psi(t)\rangle = \left(u_c(t) \hat{d}_c^\dagger + u_v(t) \hat{d}_v^\dagger \right) |0\rangle$ be the state of the system at time t the electronic density matrix reads

$$\rho_{ij}(t) = \langle \hat{d}_j^\dagger(t) \hat{d}_i(t) \rangle = u_j^*(t) u_i(t), \quad (2)$$

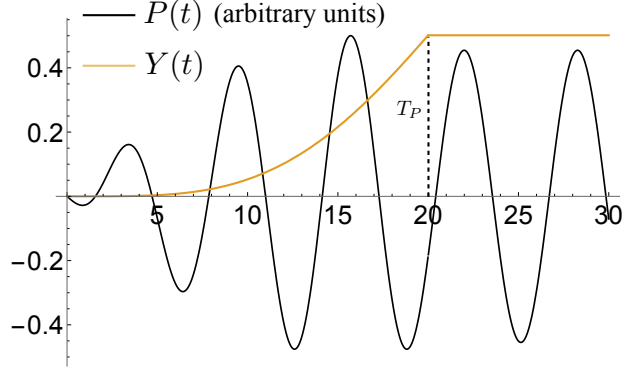


Figure 1: Time-dependent electron-hole pairs population, $Y(t)$ and polarization $P(t)$ in the simple model system described by Eq. (1). This simple model clearly show that the initial photo-excitation populates the empty bands and, at the same time, induces an oscillating contribution to the total electric field.

whereas the population of electron-hole pairs [52] reads

$$Y(t) = \langle \hat{d}_c^\dagger(t) \hat{d}_v(t) \hat{d}_v^\dagger(t) \hat{d}_c(t) \rangle - \rho_{vc}(t) \rho_{cv}(t) = \rho_{cc}(t)(1 - \rho_{vv}(t)). \quad (3)$$

For an initially filled valence band and a coherent pump field $E(t) = E_0 \sin \omega_0 t$ the time-dependent amplitudes $u_j(t)$ can easily be worked out in the rotating wave approximation [53] and they read

$$u_c(t) = -\frac{2iE_0D}{\sqrt{\Omega^2 + 4E_0^2|D|^2}} e^{-i\Omega t/2} e^{-i\epsilon_c t} \sin\left(\frac{\sqrt{\Omega^2 + 4E_0^2|D|^2}}{2} t\right), \quad (4a)$$

$$u_v(t) = i e^{i\Omega t} e^{-i\epsilon_v t} \frac{d}{dt} e^{i\epsilon_c t} \frac{u_c(t)}{E_0 D}, \quad (4b)$$

where we have defined $\Omega = \omega_0 - \epsilon_c + \epsilon_v$. If the pump is switched off at time T_P then for times $t > T_P$ we simply have $u_j(t) = u_j(T_P) e^{-i\epsilon_j(t-T_P)}$. In Fig. 1 we show the polarization of the system $P(t) = D\rho_{cv}(t) + D^*\rho_{vc}(t)$ as well as the population of electron-hole pairs $Y(t)$ for $\epsilon_c - \epsilon_v = E_g$, $DE_0 = 0.1E_g$, $\Omega = 0$ and $T_P = 20$; energies are in units of the gap E_g and times are in units of $1/E_g$.

During pumping the laser transfers coherence to the system and after pumping, i.e., for times $t > T_P$, the polarization oscillates coherently. Although $Y(t)$ attains a constant value the system is not in a quasi-thermal nor in a quasi-stationary state. This is

the so called *coherent* regime and it can last for up to few hundreds of femtoseconds. Decoherence mechanisms typically due to electron-phonon scattering are responsible for a damping of the polarization which eventually vanishes. This is the *incoherent* regime; the system can be described by a quasi-stationary density matrix. For a more detailed discussion see Ref. [54].

2.2. The paradigmatic case of the carrier lifetimes. Are they really intrinsic quantities?

One of the common belief in time-resolved experiments is that the pump pulse produces an *ideal excited state*. What is this? It is an intrinsic excited state of system, that is independent on the excitation field.

This aspect is very relevant to the physics of the material and to its potential application as technological device. This can be understood with a simple example. Imagine you need to device a system where the carrier relaxation is super-fast. Then you use TR-ARPES to detect the relaxation time of carriers pumped in the conduction bands. One paradigmatic example is described in Ref.[55] where, by using Time-Resolved two-photon Photoemission (2PPE) it was deduced an ultrafast relaxation time $\tau_f \sim 40$ fs of the photo-induced carriers.

The authors, however, interpreted this fast decay as due to intrinsic scattering mechanisms of the material, peculiar of the specific excited state triggered by the laser pulse. Theoretically this corresponds to use the so called Relaxation Time Approximation[56] and reads:

$$\frac{d}{dt} f_i(t) = \gamma_i^{EQ} [f_i(t_{th}) - f_i(t)], \quad (5)$$

with $f_i(t)$ the occupation of the level i , t_{th} the thermalization time where the occupations are supposed to follow a Fermi distribution with a given temperature, and γ_i^{EQ} the *equilibrium* lifetimes computed with the presence of photo-excited carriers.

Eq. (5) is often used as it allows to calculate the lifetimes once for all. This is a giant simplification that speeds up enormously the simulations. At the same time Eq. (5) conveys the message that the out-of-equilibrium dynamics is dictated by equilibrium quantities with the pump laser pulse just promoting carriers in the conduction bands.

This is not true at all, as it was demonstrated in Ref.[57]. In this work the authors show that the full carriers equation of motion can be reduced to a non-linear equation for the carriers occupations that, however, differ from Eq. (5):

$$\frac{d}{dt} f_i(t) = \frac{d}{dt} f_i(t) \Big|_{pump} + \frac{d}{dt} f_i(t) \Big|_{relax}. \quad (6)$$

In Eq. (6) $\frac{d}{dt} f_i(t) \Big|_{pump}$ is the driving term, written in terms of the pump laser pulse. $\frac{d}{dt} f_i(t) \Big|_{relax}$ is instead the scattering term, induced, for example by the scattering with the other electrons and/or phonons.

Therefore, at difference the RTA, Eq. (6) describes also the excitation process that, in Eq. (6) is replaced with an *ad-hoc* ansatz on the photo-excited initial populations. Indeed from Ref.[57, 58, 59] we know that

$$\frac{d}{dt} f_i(t) \Big|_{relax} = -\gamma_i^{(e)}(t) f_i(t) + \gamma_i^{(h)}(t) (1 - f_i(t)), \quad (7)$$

with $\gamma^{(e/h)}$ representing the electron/hole NEQ lifetimes. A crucial aspect of Eq. (7) is the occupations and lifetimes are time-dependent. It is natural to ask, then, to what extent $\gamma_i^{(e/h)}(t)$ are different from their equilibrium counterpart.

In Fig.2 the time-dependent averaged lifetimes (defined in Ref.[57]) at the L and L' high-symmetry points, $\bar{\gamma}_{L/L'}(t)$ of bulk Silicon are shown together with the equilibrium value.

The first striking result is that, while the equilibrium lifetime is the same at the L and L' point (the two points are one the rotated of the other) the NEQ lifetimes are not. This is due to the fact that the laser field breaks the rotational symmetry and induces a different population at the L and L' points. This, in turn, induce different NEQ lifetimes. A similar mechanism has been discussed in Ref.[60] and Ref.[61]. It is also remarkable that the NEQ lifetimes at the L' points becomes negative at early times. This is due to the fact that carriers are injected by the experimental laser only in the L point. A negative lifetime is sign of a super fast transfer of carriers from L to L' . This fast process, that is entirely due to a symmetry restoring dynamics, has been erroneously interpreted in Ref.[55] as an intrinsic process. Instead the simulations revealed that it is instead entirely due to the experimental setup.

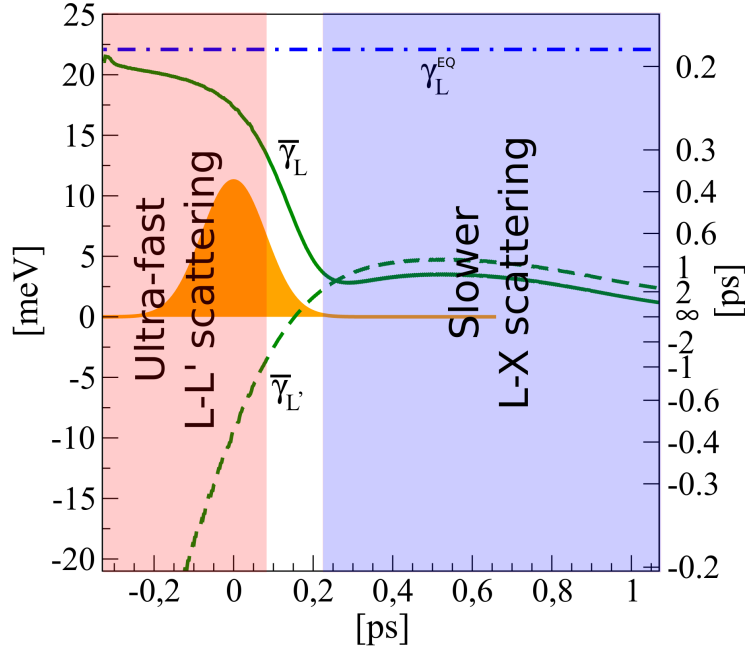


Figure 2: Time-dependent carrier lifetimes $(\bar{\gamma}_{L/L'}(t))$ compared with the equilibrium value (γ_L^{EQ}) in bulk Silicon. From Ref.[57].

After the laser pulse the two NEQ lifetimes quickly tend to the same value restoring the rotation invariance. When the full relaxation is achieved the lifetimes converge to a value that firmly remains below the equilibrium value. This demonstrates that the TR-ARPES induces effects whose interpretation must include the photo-excitation process.

3. Interacting electrons: Hamiltonian and potentials

The theoretical description of the TR-ARPES experiments is bound to a correct definition of the different quantum objects involved in the dynamics. These objects can have an entire electronic character (plasmons, excitons...) or an independent bosonic character, like phonons. In case one is interested in photoluminescence also photons must be treated quantum mechanically [59]. In this work we restrict the description to a classical treatment of the electromagnetic field, replaced by the macroscopic external one.

We start, therefore, from a general non relativistic Hamiltonian describing a system of interacting electrons moving under the action of an external electromagnetic field and of the internal electron–nucleus interaction. We will discuss in the following how this Hamiltonian can be simplified by using an *ab-initio* approach and/or approximating some of its components.

This time dependent Hamiltonian can be split in the sum of a static, equilibrium term perturbed by the external time–dependent potential:

$$\hat{H}(t) = \hat{H}^{eq} + \hat{V}(t). \quad (8)$$

The external term, \hat{V} is the one describing the interaction with the external electromagnetic field and will be discussed shortly. The equilibrium part of $\hat{H}(t)$ is composed by free terms plus interaction potentials:

$$\hat{H}^0 = \int d\mathbf{r} \hat{\psi}^\dagger(\mathbf{r}) \hat{\psi}(\mathbf{r}) h(\mathbf{r}) + \hat{H}_p, \quad (9a)$$

$$\hat{H}_{\text{int}} = \hat{H}_{e-e} + \hat{H}_{e-p}. \quad (9b)$$

Eq.(9a) represents the free electron and phonon terms. The first is written in terms of electronic field operators $\hat{\psi}$. These can be expanded in a given orthonormal single–particle basis:

$$\hat{\psi}(\mathbf{r}) = \sum_i \varphi_i(\mathbf{r}) \hat{c}_i. \quad (10)$$

Thanks to Eq. (10) Eq.(9a) becomes

$$\hat{H}^0 = \sum_i \epsilon_i \hat{c}_i^\dagger \hat{c}_i + \sum_\mu \omega_\mu \hat{b}_\mu^\dagger \hat{b}_\mu, \quad (11)$$

with \hat{c}_i^\dagger and \hat{b}_μ^\dagger electron and phonon creation operators.

The electron–phonon interaction term definition easily follow in the \hat{b} , \hat{c} representation:

$$\hat{H}_{e-p} = \sum_{ij\mu} g_{ij}^\mu \hat{c}_i^\dagger \hat{c}_j \left(\hat{b}_\mu + \hat{b}_\mu^\dagger \right), \quad (12)$$

with g_{ij}^μ the electron–phonon matrix elements [62, 63].

The electron–electron interaction is readily written in terms of electronic fields

$$\hat{H}_{e-e} = \frac{1}{2} \int \mathbf{r}\mathbf{r}' \hat{\psi}^\dagger(\mathbf{r}) \hat{\psi}^\dagger(\mathbf{r}') v(\mathbf{r} - \mathbf{r}') \hat{\psi}(\mathbf{r}') \hat{\psi}(\mathbf{r}), \quad (13)$$

with $v(\mathbf{r} - \mathbf{r}')$ the bare Coulomb potential. Eq. (13) can be further expanded in the reference basis by using Eq. (10)

$$\hat{H}_{e-e} = \sum_{ijkl} v_{ijkl} \hat{c}_i^\dagger \hat{c}_j^\dagger \hat{c}_k \hat{c}_l. \quad (14)$$

The last term to be explicitly written is the interaction with the external electromagnetic field. As the light–matter interaction is quadratic in the fermionic operators, the most general time–dependent potential reads

$$\hat{V}(t) = \sum_{ij} V_{ij}(t) \hat{c}_i^\dagger \hat{c}_j. \quad (15)$$

In Eq. (15) $V_{ij}(t)$ is the matrix element of the single particle operator $\hat{V}(\mathbf{r}, t) = \mathbf{A}(\mathbf{r}, t) \cdot \hat{\mathbf{j}}(\mathbf{r}, t)$ between the basis states i and j . Here $\mathbf{A}(\mathbf{r}, t)$ is the vector potential of the external electromagnetic field and $\hat{\mathbf{j}}(\mathbf{r}, t) = [\hat{\mathbf{v}} \delta(\hat{\mathbf{r}} - \mathbf{r}) + \delta(\hat{\mathbf{r}} - \mathbf{r}) \hat{\mathbf{v}}]/2$ the current density operator, with $\hat{\mathbf{v}} = \hat{\mathbf{p}} + \mathbf{A}(\hat{\mathbf{r}}, t)$. In this work we assume to be in the dipole approximation, where $\mathbf{A}(\mathbf{r}, t) = \mathbf{A}(t)$ and the coupling with the external field can be also expressed as $\hat{V}(\mathbf{r}, t) = \mathbf{E}(t) \cdot \hat{\mathbf{r}}$, with $\mathbf{E}(t)$ the external field.

3.1. The reference *ab-initio* system

In the previous section we have expanded the field operators in an arbitrary orthonormal basis. In practical calculations, however, the basis must be specified. In solids the index $i = n\mathbf{k}\sigma$ comprises a band-index n , a quasi-momentum \mathbf{k} and a spin orientation σ . This is the basis of Bloch states and it is particularly suited for crystals. In finite systems like atoms and molecules a more convenient basis could be made of Slater-type orbitals, Gaussian-type orbitals, etc.

The key property of this basis is that, by definition, it diagonalizes the single-particle and free Hamiltonian and defines the electronic single-particle energies ϵ_i . Thus the choice of the basis and reference single-particle Hamiltonian is crucial to embody some level of correlation already at the independent-particle level. The question, now, is how to choose this basis. There are several options:

- *Hartree–Fock* basis. This is accurate for atoms and small molecules where correlation represents a minor correction and the physics is dominated by exchange interactions.
- *Density–Functional Theory* basis. HF is not a good approximation, in general, for more complex, or correlated, materials, since HF completely neglects electronic correlation. A better starting point for extended systems is the Hamiltonian coming from Density-Functional Theory (DFT) where the self-energy is replaced by the static and local Kohn-Sham (KS) potential V^{KS} .

In the DFT case the single particle Hamiltonian appearing in Eq. (9) becomes:

$$\hat{h}(\mathbf{r}) = \hat{T}_e + \hat{V}_n(\mathbf{r}) + \hat{V}^{KS}[\rho(\mathbf{r})](\mathbf{r}). \quad (16)$$

Despite the exact V^{KS} potential is not known, simple and reliable approximations exist, in particular the so called Local–Density Approximation (LDA) and the Generalized–Gradient Approximation (GGA).

When the reference, single–particle Hamiltonian, is chosen to be Eq. (16) the whole MBPT machinery is labeled as equilibrium *ai-MBPT*, *ab-initio* Many–Body Perturbation Theory.

If electronic states can be taken from DFT, in the *ai-MBPT*, phonons, needed to write Eq. (12), are taken from Density Functional Perturbation Theory (DFPT)[64, 65]. The procedure to embody in the Eq. (12) the DFPT phonon energies and electron–phonon matrix elements is more involved than the electronic case. It is, indeed, not possible to correct the bare phonon Hamiltonian like in Eq. (16). Nevertheless it is possible to formally define families of diagrams that can be approximated by using DFPT, like described in Ref.[62].

3.2. A model Hamiltonian

It is not always possible to use the full Hamiltonian as the *ab-initio* MBPT scheme can turn very demanding forcing to use specific approximations. In order to investigate more advanced phenomena and get inspiration for extensions of the *ab-initio* scheme we have often used model Hamiltonian.

The model Hamiltonian considered in this work is a one-dimensional tight-binding insulator of \mathcal{L} sites, with one valence band $i = v$ and one conduction band $i = c$ separated by a direct gap ϵ_g [66]. Since the formation of excitons is due to the attraction between a valence hole and a conduction electron we discard the Coulomb interaction between electrons in the same band. For simplicity we also discard spin. By denoting with $\mathbf{k} = k$ the one-dimensional momentum and by $\epsilon_{i\mathbf{k}}^{\text{qp}} \equiv \epsilon_{i\mathbf{k}}$ the band dispersion, the Hamiltonian of the insulator reads

$$\hat{H}_{\text{model}}^{\text{eq}} = \sum_k (\epsilon_{vk} \hat{v}_k^\dagger \hat{v}_k + \epsilon_{ck} \hat{c}_k^\dagger \hat{c}_k) - U \sum_k \hat{c}_k^\dagger \hat{c}_k + \frac{U}{\mathcal{L}} \sum_{k_1 k_2 q} \hat{v}_{k_1+q}^\dagger \hat{c}_{k_2-q}^\dagger \hat{c}_{k_2} \hat{v}_{k_1}, \quad (17)$$

where $\hat{c}_{v\mathbf{k}} \equiv \hat{v}_k$ and $\hat{c}_{c\mathbf{k}} \equiv \hat{c}_k$ annihilates an electron of momentum k in the valence band respectively, and U is the short-range interband repulsion. The second term represents the interaction of a conduction electron with the positive background in the valence band. For this model the ground state is obtained by filling all single-particle valence states with one electron. Therefore the number of protons is equal to the number of valence electrons \mathcal{L} in the ground state. Since we will use Eq. (17) to study either the early stage of the long-time regime of the pump-induced dynamics Eq. (17) ignores phonon-relaxation and decoherence.

4. Ab-Initio Many-Body Perturbation Theory

The Hamiltonian Eq. (8) is composed of a static term, \hat{H}^{eq} plus a time-dependent perturbation, $\hat{V}(t)$. The solution of the Many-Body problem for \hat{H}^{eq} already represents a challenging task and it requires some fundamental approximations that we will briefly review in the next sections. At the same time the equilibrium problem already allows to introduce some key concepts that will remain valid out-of-equilibrium. The whole theoretical scheme, indeed, even if turning more complicate because of the explicit time-dependence of the perturbation, preserves the conceptual structure that emerges clearly at the equilibrium.

The first and fundamental concept that emerges from the solution of the equilibrium problem is the concept of trajectory. All excited state properties of the many-body system can be deduced from the dynamics of an electron traveling in the fully interacting

material. This travel is described, mathematically, from the single-particle Green's function, that in equilibrium system, can be written as a time-ordered object [67, 68, 69, 53]:

$$G_{ij}(t, t') = \theta(t - t') G_{ij}^>(t, t') + \theta(t' - t) G_{ij}^<(t, t'). \quad (18)$$

The physical interpretation of Eq. (18) is given by the two components that governs the dynamics in the different time orderings: the greater ($G^>$) and lesser ($G^<$) Green's function (GF) which describe the propagation of an added electron and hole respectively. From the definition of G it follows that

$$G_{ij}^>(t, t') = -i \left\langle \hat{c}_i(t) \hat{c}_j^\dagger(t') \right\rangle, \quad (19a)$$

$$G_{ij}^<(t, t') = i \left\langle \hat{c}_j^\dagger(t') \hat{c}_i(t) \right\rangle. \quad (19b)$$

where operators depend on time according to the Heisenberg picture and the average $\langle \dots \rangle$ is performed over the initial ground state (or the initial many-body density matrix at finite temperature).

At the equilibrium the description of the electronic motion simplifies enormously as the time-ordered Green's function G depends only on the time difference:

$$G_{ij}(t, t') \xrightarrow{\text{equilibrium}} G_{ij}(t - t'). \quad (20)$$

In practice this means that the GF can be Fourier transformed. This allows to expand it in a form, Lehmann representation, which clearly shows that connection between trajectories and excited state properties. Indeed if we take Eq. (18) and the its two components, Eq. (19), and consider the zero-temperature case to simplify the math, it is straightforward to realize that

$$G_{ij}(\omega) = \sum_I \frac{f_i^I (f_j^I)^*}{\omega - \tilde{\epsilon}_I + i0^+ \text{sign}(\tilde{\epsilon}_I - \mu)}, \quad (21)$$

with μ the chemical potential and

$$\tilde{\epsilon}_I = \begin{cases} E_0^N - E_I^{N-1} & \text{when } \tilde{\epsilon}_I < \mu, \\ E_I^{N+1} - E_0^N & \text{when } \tilde{\epsilon}_I \geq \mu. \end{cases} \quad (22)$$

In Eq. (21)

$$f_i^I = \begin{cases} \langle N-1, I | \hat{c}_i | N, 0 \rangle & \text{when } \tilde{\epsilon}_I < \mu, \\ \langle N, 0 | \hat{c}_i | N+1, I \rangle & \text{when } \tilde{\epsilon}_I \geq \mu. \end{cases} \quad (23)$$

Eq. (21)–(23) clearly shows that the knowledge of the frequency dependent single-particle GF is directly connected to the exact one-body excitation energies of the system.

Now the problem is how to calculate G . In MBPT G is the solution of a set of integro-differential equations that can be derived by using two different, although equivalent, paths. One is based on the standard diagrammatic technique [70] which constructs approximations for the different terms of the theory by using a geometrical and graphical approach. An alternative approach is based instead on the equation of motion approach [71]. This method leads, both in the equilibrium and the out-of-equilibrium regimes, to a closed set of integro-differential equations that at the equilibrium are known as Hedin's equations [72].

Both approaches lead to an equation of motion for G written in terms of an electronic self-energy, Σ . This is the Dyson equation

$$\underline{G}(t-t') = \underline{g}(t-t') + \int dt_1 dt_2 \underline{g}(t-t_1) \underline{\Sigma}(t_1-t_2) \underline{G}(t_2-t'), \quad (24)$$

where g is the bare GF and Σ the time-ordered (correlation) self-energy respectively. In Eq. (24) we used underlined quantities to indicate matrices in the (ij) basis.

If now we take into account the equation of motion of g , i.e.,

$$\left[i \frac{d}{dt} - \underline{h} \right] \underline{g}(t, t') = \delta(t, t') \underline{1}, \quad (25)$$

we can rewrite the Dyson equation as the following integro-differential equation

$$\left[i \frac{d}{dt} - \underline{h} \right] \underline{G}(t-t') = \delta(t-t') \underline{1} + \int d\bar{t} \underline{\Sigma}(t-\bar{t}) \underline{G}(\bar{t}-t'), \quad (26)$$

that will be particularly useful when we will move to the non-equilibrium regime. Eq. (26) comes together with its adjoint [71].

Eq. (24) makes clear that all the complexity of the many-body system is embodied in the self-energy operator. In some sense this quantity plays the same role of exchange-correlation potential of DFT that, if exact provides the exact ground state density, but

that, in practice, is approximated. Compared to DFT the great advantage of MBPT is that it offers a systematic way to approximate $\underline{\Sigma}$, since its exact expression in terms of G and the bare e–e and e–p interaction is, in principle, known [71, 63]. In practice it involves the definition of very involved and inter-connected objects (like the vertex function) that impose the adoption of approximations. Thanks to the perturbative nature of the MBPT scheme it is always possible to ground these approximations on physical grounds.

4.1. Quasiparticles and lifetimes

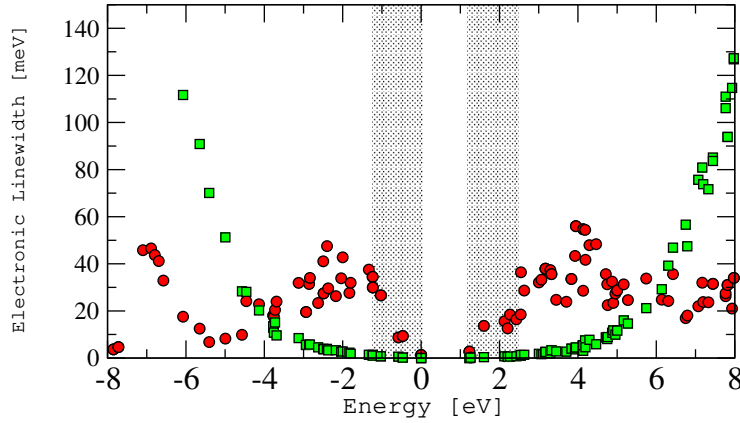


Figure 3: Quasi-particle lifetimes in bulk Silicon. From Ref. [58]. Lifetimes are computed using Eq. (30) with the electron–electron (boxes) and electron-phonon self-energy (circles).

The most elemental concept to use in order to show the power of the MBPT scheme is the quasiparticle (QP) concept. In DFT and in the KS scheme any electron is accommodated on the levels corresponding to the eigenvalues of the KS Hamiltonian. These eigenvalues are, by construction, real. The MBPT gives a different and alternative picture to it by distinguishing the different physical mechanisms that are responsible for the dressing of the bare electron: classical, exchange and, finally, correlation effects. All these effects are embodied in the self-energy and correspond to specific approximations to it.

In order now to understand the effects induced by the frequency dependence of the correlated self-energy we can use Eq. (24) and approximate g , G and $\underline{\Sigma}$ to be diagonal in

the i, j indexes. This allow a simple, analytic expression for the Dyson equation written in frequency space

$$G_i(\omega) = g_i(\omega) [1 + \Sigma_i(\omega) G_i(\omega)]. \quad (27)$$

From Eq. (21) we now know that

$$g_i(\omega) = \frac{1}{\omega - \epsilon_i^0 + i0^+ \text{sign}(\epsilon_i^0 - \mu)}, \quad (28)$$

with ϵ_i^0 the bare, reference energies. Taking inspiration from Eq. (28) we can introduce the quasiparticle approximation by assuming that

$$G_i^{QP}(\omega) \approx \frac{Z_i}{\omega - \epsilon^{QP}}. \quad (29)$$

If we plug Eq. (29) into Eq. (27) we obtain

$$\epsilon_i^{QP} = \epsilon_i^0 + Z_i \Sigma_{ii}(\epsilon_i^{QP}), \quad (30)$$

with $Z_i = (1 - \partial_\omega \Sigma|_{\omega=\epsilon_i^0})^{-1}$ the renormalization factors. Eq. (30) contains a crucial difference compared to DFT and/or HF: the QP energies ϵ^{QP} are complex. Physically we have that the real part of the QP energy corresponds to the renormalization of the single-particle energy levels, while the imaginary part provides the QP width, that is the energy indetermination caused by quantistic effects.

For reference in Fig.3 we show the QP lifetimes (proportional to the inverse line-widths) in bulk Silicon from Ref.[58]. Both the electronic and the phonon-induced lifetimes are reported. Those are calculated in the GW approximation that will be shortly reviewed in Section 4.1.1.

4.1.1. Specific Self-Energy approximations

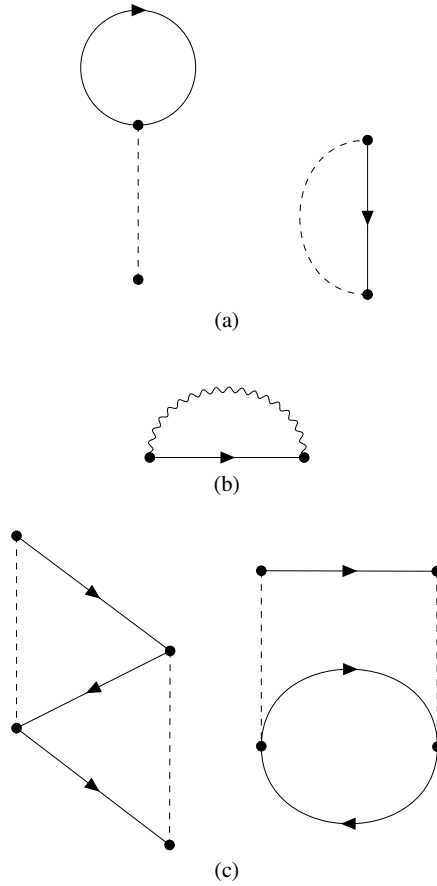


Figure 4: Diagrammatic form of the self-energy approximations discussed in this work. We have the: (a) Hartree (left) and Fock (right), (b) GW , (c) second-Born approximations. In the GW approximation the wiggled propagator represent either the screened electronic interaction or the phonon propagator (see text). More information can be found, for example, in Ref.[53, 58, 59].

Hartree and Hartree Fock. At the lowest order of perturbation theory the two-body Coulomb interaction appearing in Eq. (14) produces two terms, diagrammatically

represented in Fig.4(a):

$$\Sigma_{ij}^{Hartree} = -2i \sum_{\bar{m}\bar{n}} v_{i\bar{m}\bar{n}j} G_{\bar{n}\bar{m}}(t, t^+), \quad (31a)$$

$$\Sigma_{ij}^{Fock} = i \sum_{\bar{m}\bar{n}} v_{i\bar{m}j\bar{n}} G_{\bar{n}\bar{m}}(t, t^+). \quad (31b)$$

The first term is the Hartree or classical term with the factor 2 due to the spin summation. It can be easily visualized that it corresponds to solution of the Poisson equation by writing it in real space

$$\Sigma^{Hartree}(\mathbf{r}, \mathbf{r}') = -i\delta(\mathbf{r} - \mathbf{r}') \int d\bar{\mathbf{r}} v(\mathbf{r} - \bar{\mathbf{r}}) G(\bar{\mathbf{r}}, \bar{\mathbf{r}}; t, t^+), \quad (32)$$

with

$$G(\mathbf{r}, \mathbf{r}'; t, t') = \sum_{ij} \phi_i(\mathbf{r}) (\phi_j(\mathbf{r}'))^* G_{ij}(t, t'). \quad (33)$$

Eq. (32) clearly shows that it represents the electrostatic potential generated by the electronic density, $\rho(\bar{\mathbf{r}}) \equiv -iG(\bar{\mathbf{r}}, \bar{\mathbf{r}}; t, t^+)$. A similar analysis can be done for the Fock term that reveals that it corresponds to exchange interaction caused by the anti-symmetric properties of the electronic states. As at equilibrium the GF depend only on the time difference the HF self-energy is static, $\underline{\Sigma}^{HF} = \underline{\Sigma}^{Hartree} + \underline{\Sigma}^{Fock}$.

The GW approximation: the electronic case. All terms that go beyond the HF approximation are commonly defined as correlation terms. The most striking difference with HF is that, even at equilibrium, the correlation self-energy is frequency dependent reflecting the retardation effects caused by the interaction.

The general diagrammatic form of the *GW* approximation is shown in Fig.4(b) and it can be applied to either the electronic or the phonon mediated interaction.

We start, here, from the electronic case. As discussed both using the geometric, diagrammatic and the equation-of-motion approaches the most elemental excitation that is not included in the HF approximation is the electron-hole pair creation. In practice it is possible to demonstrate that in the high density limit [70] all correlation effects are exactly described by the charge oscillations described by the electronic response function, $\chi(\mathbf{r}, \mathbf{r}'; t - t')$. The physical meaning of the response function can be easily visualized by noticing that it is the same object entering the Kubo equation describing, within linear-response, the reaction of a system to weak external perturbation.

Let's, indeed, consider the potential defined in Eq. (15) and let's also assume that \hat{V} is so weak to be possible to be treated perturbatively. At the first order this potential will induce a change in the density described by the Kubo equation

$$\delta\rho(\mathbf{r}, t) = \int dt' d\mathbf{r}' \chi(\mathbf{r}, \mathbf{r}'; t - t') V(\mathbf{r}', t'). \quad (34)$$

From Eq. (34) we can also introduce an alternative definition of the response function, written as functional derivative,

$$\chi(\mathbf{r}, \mathbf{r}'; t - t') = \frac{\delta\rho(\mathbf{r}, t)}{\delta V(\mathbf{r}', t')}. \quad (35)$$

The next step we have to do in order to connect χ to correlation effects can be formally done [73] by using a variational approach. Here, however, we follow a simpler approach entirely based on the Eq. (34). Indeed if we now we consider as perturbing potential $V(\mathbf{r}', t')$ the classical field generated by a moving charge we readily see that Eq. (34) describes the interaction of this charge with the electrons present in the material in terms of a modified interaction

$$\begin{aligned} W(\mathbf{r}, \mathbf{r}'; t - t') &\equiv v(\mathbf{r} - \mathbf{r}') \delta(t - t') + \\ &\int d\bar{\mathbf{r}} \bar{v}(\mathbf{r} - \bar{\mathbf{r}}) \chi(\bar{\mathbf{r}}, \mathbf{r}'; t - t') v(\mathbf{r} - \mathbf{r}') = \\ &\int d\bar{\mathbf{r}} \epsilon^{-1}(\bar{\mathbf{r}}, \mathbf{r}'; t - t') v(\mathbf{r} - \mathbf{r}'). \end{aligned} \quad (36)$$

Eq. (36) is the formal definition of the longitudinal screened interaction [71] that can also be written as the product of the inverse dielectric function ϵ^{-1} times the bare Coulomb interaction. If we now consider the Fock self-energy we see that it represents exchange scatterings mediated by the bare e-e interaction. By using the simple dielectric argument used to derive Eq. (36) we deduce that the first effect of correlation will be transform the bare e-e interaction, in the Fock self-energy, in W . Thus we have that

$$\underline{\Sigma}_{ij}^{Fock} \Longrightarrow \underline{\Sigma}_{ij}^{GW} = i \sum_{\bar{m}\bar{n}} \int d\omega' W_{i\bar{m}j\bar{n}}(\omega - \omega') G_{\bar{n}\bar{m}}(\omega'). \quad (37)$$

It is worth to remind the Eq. (37) is exact in the homogeneous electron gas in the limit of high density. A condition, however, hardly satisfied in realistic materials.

The GW approximation: the phononic case and the Fan approximation. When the W propagator is replaced by the phonon propagator Eq. (37) defines another popular approximation very commonly used to describe electron–phonon effects [63]. In this case $W \rightarrow D$:

$$D_\mu(t, t') = \theta(t - t') D_\mu^>(t, t') + \theta(t' - t) D_\mu^<(t, t'), \quad (38)$$

with

$$D_{ij}^>(t, t') = -i \langle \hat{q}_\mu(t) \hat{q}_\mu(t') \rangle, \quad (39a)$$

$$D_{ij}^<(t, t') = i \langle \hat{q}_\mu(t') \hat{q}_\mu(t) \rangle, \quad (39b)$$

and $\hat{q} = (\hat{b}_\mu + \hat{b}_\mu^\dagger) / \sqrt{2}$. When W is replaced with D in Eq. (37) we get the Fan self–energy:

$$\Sigma_{ij}^{Fan}(t, t') = i \sum_{kl} \sum_{\mu} (g_{ik}^\mu)^* g_{jl}^\mu D_\mu(t, t') G_{kl}(t', t'). \quad (40)$$

At the equilibrium Σ and D depend only on the time difference, as in Eq. (37).

The Fan self–energy, plus the Debye–Waller correction [63] has been applied extensively to investigate the effect of the electron–phonon interaction on the electronic and optical properties of a wealth of materials. One of the first applications was the simulation of the finite temperature properties of extended systems [74].

The second–Born (2B) approximation. The driving mechanism that motivates the success of the GW approximation is the description in terms of dielectric screening, χ . In systems composed of many electrons this is the most elemental process that is also directly connected to the electrostatics of the material. When, however, the system is small and there are not many electrons collective excitation, as those needed to build up screening, are not possible or less important. In these systems it is much more important to take correctly into account exchange diagrams and avoid self–interaction errors.

For these kind of systems where screening is not dominant a well–known approximation is the second–Born (2B). Diagrammatically this is represented by Fig.4(c) and it is composed of two terms. The first (right diagram) is in common with the GW approximation and corresponds to the lowest order diagram. The second (left diagram) is

the exchange and, from the GW perspective, represents the lowest order vertex of the self-energy.

The 2B self-energy can be written as

$$\Sigma_{ij}^{2B}(t, t') = \sum_{nmpqsr} v_{irpn} w_{mqsj} G_{nm}(t, t') G_{pq}(t, t') G_{sr}(t', t), \quad (41)$$

where

$$w_{imnj} \equiv v_{imnj} - v_{imjn}. \quad (42)$$

4.2. Neutral excitation: plasmons and excitons

The response function $\chi(\mathbf{r}, \mathbf{r}'; \omega)$ is formally defined via the Kubo relation, Eq. (34), which can be rewritten in terms of a density variation, Eq. (35). The Kubo equations, is however, a very general tool to describe the variation of any observable given the external perturbation.

In order to connect the response function to the macroscopic, observable, physics we need however to carefully define the perturbing field. Indeed in realistic materials we have three possibilities:

- (a) The perturbing field is the external, bare field,
- (b) The perturbing field is the *total* field, i.e. the sum of the external plus the induced fields,
- (b) The perturbing field is the *total* and *macroscopic* field corresponding to the macroscopic component of the total field.

Each of the above definitions of the external perturbation defines, via the Kubo relation, a corresponding response function.

4.2.1. Potentials and response functions

Let's start from case (a). In this case the definition of the perturbing field is simple and Kubo equation reduces to Eq. (34) and Eq. (35). We have, then, that upon application of the external perturbation the system will induce a variation of the density. If

now we use simple electrostatic arguments we see that this variation will correspond to a variation of Hartree potential, solution of Poisson equation:

$$\delta\Sigma^{Hartree}(\mathbf{r}, t) = \int d\mathbf{r}' v(\mathbf{r} - \mathbf{r}') \delta\rho(\mathbf{r}', t), \quad (43)$$

Eq. (43) defines the *induced potential*. This, physically, corresponds to the potential induced by the external perturbation.

At this point we have two potentials: an external $V(\mathbf{r}, t)$, time-dependent and spatially homogeneous, and a microscopic, $\delta\Sigma^{Hartree}(\mathbf{r}, t)$, time-dependent but with microscopic components.

In an optical absorption experiment the scattered light measured corresponds, for obvious reasons, to the total and *macroscopic* potential. The total potential is the sum of V and $\delta\Sigma^{Hartree}$. In the macroscopic component, V_M^{tot} is spatially averaged as the external potential is, by definition, macroscopic:

$$V^{tot}(\mathbf{r}, t) = V(\mathbf{r}, t) + \delta\Sigma^{Hartree}(\mathbf{r}, t), \quad (44a)$$

$$V_M^{tot}(\mathbf{r}, t) = V(\mathbf{r}, t) + \frac{1}{\Omega} \int d\mathbf{r} \delta\Sigma^{Hartree}(\mathbf{r}, t), \quad (44b)$$

with Ω the crystal volume.

We have now the formal definition of the three possible perturbing fields. For each of them Eq. (34) defines a response function. In addition to χ , therefore, we have

$$\chi^{tot}(\mathbf{r}, \mathbf{r}'; t - t') = \frac{\delta\rho(\mathbf{r}, t)}{\delta V^{tot}(\mathbf{r}', t')}, \quad (45a)$$

$$\chi_M(\mathbf{r}, \mathbf{r}'; t - t') = \frac{\delta\rho(\mathbf{r}, t)}{\delta V_M^{tot}(\mathbf{r}', t')}. \quad (45b)$$

The natural question is: which one is the correct one to be used to interpret a given experiment? In the case of the optical absorption we know that the macroscopic absorption is given by

$$\epsilon_M(\omega) = \frac{1}{\langle\langle \epsilon^{-1}(\mathbf{r}, \mathbf{r}'; \omega) \rangle\rangle} = 1 - \left\langle\left\langle \int d\bar{\mathbf{r}} v(\mathbf{r} - \bar{\mathbf{r}}) \chi_M(\bar{\mathbf{r}}, \mathbf{r}'; \omega) \right\rangle\right\rangle. \quad (46)$$

Similarly the electron-energy loss spectrum is given by

$$\epsilon^{-1}(\omega) = \langle\langle \epsilon^{-1}(\mathbf{r}, \mathbf{r}'; \omega) \rangle\rangle = 1 + \left\langle\left\langle \int d\bar{\mathbf{r}} v(\mathbf{r} - \bar{\mathbf{r}}) \chi(\bar{\mathbf{r}}, \mathbf{r}'; \omega) \right\rangle\right\rangle, \quad (47)$$

where we have introduced the double brackets notation to represent a macroscopic average:

$$\langle\langle f(\mathbf{r}, \mathbf{r}') \rangle\rangle \equiv \int d\mathbf{r} d\mathbf{r}' f(\mathbf{r}, \mathbf{r}'). \quad (48)$$

From Eq. (46) and Eq. (47) it follows that we need different response function depending on the experimental setup.

A last remark is that, by following the same strategy adopted in the single-particle GF case, also χ can be represented in a Lehmann form. The form shows that the poles of χ are number conserving excitation $E_I(N) - E_0(N)$.

4.2.2. The Bethe–Salpeter equation(s)

It is well known[75] that the response function satisfies an equation named Bethe–Salpeter Equation (BSE). From Eq. (45) is evident that we have more than one BSE depending on which response function (observable) we are interested in.

Let's take as example χ . χ can be derived, in the framework of MBPT, from the four point electron–hole propagator $\chi_{ijkl}(\omega)$. This is defined by expanding Eq. (35) in the reference basis

$$\chi_{ijkl}(t-t') \equiv \frac{\delta \rho_{ij}(t, t^+)}{\delta V_{lk}(t')}. \quad (49)$$

While χ is a two points function in real space χ is a four point function in the single-particle basis [71].

The equation of motion for χ follows exactly the same path we outlined in the case of the single-particle GF, Sec. 4. We can use either the diagrammatic path or the equation of motion approach. From Eq. (49) we observe that $-iG_{ij}(t, t^+) = \rho_{ij}(t)$, with $\underline{\rho}$ the density matrix. Now, the equation of motion for ρ follows from the equal time contraction of the Eq. (26). Let's consider, for the moment, just the HF contribution to the self-energy operator. This term is time independent and simplifies the math

$$\frac{d}{dt^-} \rho(t) = -i \left[\underline{h} + \underline{\Sigma}^{Fock}(t) + \underline{V}^{tot}(t), \underline{\rho}(t) \right]. \quad (50)$$

In Eq. (50) Σ^{HF} is the time-dependent HF self-energy, which is functional of the density matrix itself, see Eq. (31). From Eq. (50) the equation of motion for χ follows

easily.

$$\frac{d}{dt}\underline{\underline{\chi}}(t-t') = -i \left[\underline{\underline{h}}, \underline{\underline{\chi}}(t-t') \right] - i \left[\underline{\underline{K}}^{Fock} \circ \underline{\underline{\chi}}(t, t') + \frac{\delta \underline{\underline{V}}^{tot}(t)}{\delta \underline{\underline{V}}(t')}, \underline{\underline{\rho}}_0 \right], \quad (51)$$

with

$$\delta \underline{\underline{\Sigma}}^{Fock} = \underline{\underline{K}}^{Fock} \circ \delta \underline{\underline{\rho}}(t) \Big|_{\rho=\rho_0}. \quad (52)$$

Eq. (51) is the BSE for the generic response function χ . In Eq. (51) we have also introduced a short notation for matrix–matrix and matrix–vector multiplications. If M and N are two matrices and V is a vector we define

$$(M \circ V)_{pq} \equiv M_{mn}^{pq} V_{nm}, \quad (53a)$$

$$(M \circ N)_{mn} \equiv M_{rs}^{mn} N_{pq}^{rs}, \quad (53b)$$

$$[N, V]_{mn}^{pq} = -[V, N]_{pq}^{mn} \equiv N_{mi}^{pq} V_{in} - V_{mi} N_{pq}^{in}. \quad (53c)$$

In order to make explicit the last term of Eq. (51) we need to specify which polarization function we are interested in. Indeed, the final form of the BSE depends on the definition of the perturbing field. Indeed we have that

$$\frac{\delta \underline{\underline{V}}^{tot}(t)}{\delta \underline{\underline{V}}(t')} = \begin{cases} \frac{\delta \underline{\underline{\Sigma}}^{Hartree}(t)}{\delta \underline{\underline{V}}(t')} \Big|_{\rho=\rho_0} + \underline{\underline{1}} \delta(t-t') & \chi = \chi^{tot} \\ \underline{\underline{1}} \delta(t-t') & \chi = \chi_M \\ \frac{\delta \underline{\underline{V}}^{tot}(t)}{\delta \underline{\underline{V}}(t')} \Big|_{\rho=\rho_0} & \chi = \chi_M^{tot} \end{cases} \quad (54)$$

5. *Ab-Initio* Non–Equilibrium Green’s Function Theory

So far we have dealt with systems in equilibrium where the techniques of MBPT applies. This approach, however, is based on some key assumptions. The system is supposed to: (i) be time invariant, i.e. all observable depend only on time differences; (ii) be in the ground state and/or in a thermally distributed mixture of excited states.

These two assumptions clearly fail in the case where an external time–dependent perturbation is applied. When this perturbation is weak it is still possible to describe

the system in terms of the equilibrium Hamiltonian and treat the perturbation within Linear-Response regime.

In typical P&p experiments, however, the external perturbation can be arbitrary strong and the two conditions on which equilibrium MBPT is based cease to hold. Nevertheless, in this regime, it is possible to extend the Green's function approach as well as the approximations generated from MBPT. This extension is the Non-Equilibrium Green Function approach (NEGF). The NEGF scheme has been devised in the sixties and it is reviewed, for example, in Ref.[53].

5.1. NEGF and connection to observable quantities

Let's indeed consider now the action of the external perturbation of Eq. (8). The external driving field $V(t)$ breaks the invariance under time-translations. Consequently any observable acquires an explicit time dependence. Let's take as an example the HF self-energy,

$$\Sigma_{ij}^{\text{HF}}(t) = \sum_{\bar{m}\bar{n}} (v_{i\bar{m}\bar{n}j} - v_{i\bar{m}j\bar{n}}) \rho_{\bar{m}\bar{n}}(t), \quad (55)$$

whose time dependence is through $\rho_{nm}(t)$, the one-particle density matrix. We can thus define the time dependent NEQ Hamiltonian:

$$\underline{h}^{\text{neq}}(t) = \underline{h} + \underline{\Sigma}^{\text{HF}}(t) + \underline{V}(t) = \underline{h}^{\text{HF}}(t) + \underline{V}(t). \quad (56)$$

The G^{\lessgtr} functions in Eq. (19) contains a wealth of information about the non-equilibrium system. From the *equal-time* $G^<(t, t)$ we have access to the one-particle density matrix according to

$$\underline{\rho}(t) = -i\underline{G}^<(t, t), \quad (57)$$

and therefore any time-dependent average of any one-body operator $\hat{O} = \sum_{ij} O_{ij} \hat{c}_i^\dagger \hat{c}_j$ can be evaluated as:

$$O(t) = \sum_{ij} O_{ij} \left\langle \hat{c}_i^\dagger(t') \hat{c}_j(t) \right\rangle = -i \sum_{ij} O_{ij} G_{ji}^<(t, t). \quad (58)$$

Thus, $G^<(t, t)$ can be used to calculate time-dependent local densities, currents, spin-densities, spin-currents, orbital magnetic moments, dipole moments, etc. Interestingly,

for weak perturbations V the Fourier transform of $O(t)$ is peaked at the absorption energies of the equilibrium system. Hence, real-time simulations provide an alternative route to obtain different kind of response functions. Knowledge of the *off-diagonal* (in time) $G_{ij}^<(t, t')$ allows for the calculation of the time-dependent total energy [53], i.e., the average of $\hat{h}^{\text{neq}}(t)$ defined in Eq. (56):

$$E(t) \equiv \langle \hat{h}^{\text{neq}}(t) \rangle = -\frac{i}{2} \sum_{ij} \left(h_{ij}^{\text{HF}}(t) + V_{ij}(t) \right) G_{ji}^<(t, t) = -\frac{i}{4} \sum_i \left[\left(i \frac{d}{dt} - i \frac{d}{dt'} \right) G_{ii}^<(t, t') \right]_{t=t'}. \quad (59)$$

Finally, the Fourier transform of $G^{\lessgtr}(t, t')$ with respect to the relative time $t - t'$ yields the time-resolved spectral function

$$A^{\lessgtr} \left(T = \frac{t+t'}{2}, \omega \right) \equiv -i \int d(t-t') e^{i\omega(t-t')} \text{Tr}[\underline{G}^{\lessgtr}(t, t')]. \quad (60)$$

The quantity $A^<(A^>)$ is peaked at the removal (addition) single-particle energies of the system at time T and hence it can be used to address transient photo-emission spectra (inverse photo-emission spectra) as we shall see later.

Given the importance of the lesser/greater Green's functions in the characterization of a physical system we now discuss briefly how they can be calculated in practice.

5.2. From the full Kadanoff-Baym equations to the single-time evolution method

In non-equilibrium the equation of motion Eq. (26) is replaced by a coupled system of integro-differential equations for the lesser/greater Green's functions, also known as the *Kadanoff-Baym equations* (KBE) [76, 77, 78, 79, 53, 80]

$$\left[i \frac{d}{dt} \underline{1} - \underline{h}^{\text{HF}}(t) \right] \underline{G}^<(t, t') = \underline{I}^<(t, t'), \quad (61a)$$

$$\underline{G}^>(t, t') \left[-i \frac{\bar{d}}{dt'} \underline{1} - \underline{h}^{\text{HF}}(t') \right] = \underline{I}^>(t, t'), \quad (61b)$$

with collision integrals

$$\underline{I}^<(t, t') = \int_{-\infty}^{\infty} dt_1 \left[\underline{\Sigma}^<(t, t_1) \underline{G}^{\text{A}}(t_1, t') + \underline{\Sigma}^{\text{R}}(t, t_1) \underline{G}^<(t_1, t') \right], \quad (62a)$$

$$\underline{I}^>(t, t') = \int_{-\infty}^{\infty} dt_1 \left[\underline{G}^>(t, t_1) \underline{\Sigma}^{\text{A}}(t_1, t') + \underline{G}^{\text{R}}(t, t_1) \underline{\Sigma}^>(t_1, t') \right]. \quad (62b)$$

In Eq. (62) it appears the retarded/advanced component of the Green's function and self-energy. They are defined according to

$$X^R(t, t') = [X^A(t', t)]^\dagger = \theta(t - t') [X^>(t, t') - X^<(t, t')], \quad (63)$$

where X can be any other two-time correlator. The collision integrals I^{\lessgtr} encode all correlation effects via the many-body self-energy Σ_c . Since $\Sigma^{\lessgtr} = \Sigma^{\lessgtr}[G^>, G^<]$ are functionals of $G^>$ and $G^<$, Eq. (61) constitute a closed nonlinear system of integro-differential equations. We refer to this approach of tackling non-equilibrium problems as the *Non-equilibrium Green's function* (NEGF) method.

From Eqs. (61,62) it is evident that the computational cost of solving the NEGF equations scales cubically with the propagation time. For this reason the full numerical solution of the KBE has so far being limited to light atoms and diatomic molecules [81, 82, 83, 84], the homogeneous electron gas [85, 86, 87], the two-band model [88, 89, 90, 91, 92] and several model Hamiltonians for finite systems [93, 94, 95, 96, 97], lattice systems [98, 99, 100] and open systems [101, 102, 103, 104, 105, 106, 107, 108, 109].

In order to allow for first-principles NEGF simulations of complex molecules or crystals, one has to circumvent the problem of the cubic scaling. A way to drastically reduce the computational time consists in implementing the so-called Generalized Kadanoff-Baym Ansatz (GKBA) [110]. The basic idea is to collapse the KBE into a single equation for the one-particle density matrix $\rho(t) = -iG^<(t, t)$ from which one can calculate the time-dependent averages of all one-body observable. Thus, with the GKBA we loose the information brought by the off-diagonal in time Green's functions but we gain in computational efficiency.

The exact equation for $\rho(t)$, that was derived in Section 4.2.2 within the HF approximation, can be also derived within NEGF from the difference between Eq.(61a) and Eq.(61b), and reads

$$\frac{d}{dt}\underline{\rho}(t) + i \left[\underline{h}^{\text{HF}}(t), \underline{\rho}(t) \right] = -\underline{I}(t), \quad (64)$$

with

$$\underline{I}(t) \equiv \underline{I}^<(t, t) + \text{H.c.} \quad (65)$$

This is not a closed equation for ρ since the collision integral

$$\begin{aligned} \underline{I}(t) = - \int_{-\infty}^t dt' & \left[\underline{\Sigma}^<(t, t') \underline{G}^>(t', t) + \underline{\Sigma}^>(t, t') \underline{G}^<(t', t) \right. \\ & \left. + \underline{G}^<(t, t') \underline{\Sigma}^>(t', t) + \underline{G}^>(t, t') \underline{\Sigma}^<(t', t) \right]. \end{aligned} \quad (66)$$

depends on the off-diagonal in time G^{\lessgtr} both explicitly and implicitly through Σ .

According to the GKBA one can close Eq. (64) by approximating the lesser and greater Green' function as

$$\underline{G}^<(t, t') = -\underline{G}^R(t, t') \underline{\rho}(t') + \rho(t) \underline{G}^A(t, t'), \quad (67a)$$

$$\underline{G}^>(t, t') = \underline{G}^R(t, t') \underline{\bar{\rho}}(t') - \underline{\bar{\rho}}(t) \underline{G}^A(t, t'), \quad (67b)$$

where $\underline{\bar{\rho}}(t) = 1 - \rho(t)$, and the quasi-particle propagator G^R (and hence $G^A = [G^R]^\dagger$) as

$$\underline{G}^R(t, t') = -i\theta(t - t') T e^{-i \int_{t'}^t d\bar{t} h^{QP}(\bar{t})}. \quad (68)$$

For (small) finite systems the choice $h^{QP} = h^{HF}(t)$ is a good choice [111]. For extended systems, however, the lack of damping in h^{eq} prevents the system to relax. In these cases the propagator is typically corrected by adding non-hermitian terms given by the quasi-particle life-times, see Section 4.1.1. In this case the self-energy is not hermitian and the quasi-particle energy includes an imaginary part [74, 112, 113, 114, 115, 116, 117].

$$h_{ij}^{QP} = \delta_{ij} \left[\text{Re} \left(\epsilon_i^{QP} \right) + i \text{Im} \left(\epsilon_i^{QP} \right) \right]. \quad (69)$$

To summarize, Eq. (64) together with Eq. (67) and Eq. (68) constitute a closed equation of motion for ρ called *GKBA method*. The computational cost of this method scales quadratic with the propagation time (if the calculation of the self-energy does not scale worse than it), thus offering a huge gain with respect to the solution of the KBE.

Among the properties of the GKBA we mention the fulfillment of the relation $G^R - G^A = G^> - G^<$ for any choice of G^R , and the fact that Eqs. (67) become an identity in the limit $t \rightarrow t'$ since $G^R(t^+, t) = -i$. Another important feature is that the GKBA preserves the continuity equation.

There is, however, an even more important property which clarifies the physics contained in the GKBA. In the HF approximation the collision integral vanishes and

Eq. (67) are the solution of Eq. (64) provided that G^R is the HF propagator. Therefore, the more the quasi-particle picture is valid the more the GKBA is accurate. This is typically the case when the time between two consecutive collisions is smaller than the quasi-particle life-time.

The GKBA approach has been successfully applied in many contexts, including both finite and extended systems. Recent applications include the non-equilibrium dynamics [118, 119] and many-body localization [120] of Hubbard clusters, time-dependent quantum transport [117, 121, 122, 123], real-time description of the Auger decay [124], transient absorption of atoms [111, 125], ultrafast charge migration in bio-molecules [126, 127, 128, 129] and donor/acceptor dyads [130], time-resolved spectroscopy of excitonic insulators out of equilibrium [131, 132, 133], equilibrium absorption of sodium clusters [134], transient absorption [135, 136, 137] and carrier dynamics [57, 138] of semiconductors.

Below we discuss a possible next level of approximation to further reduce the computational effort of the GKBA method.

5.3. The Markovian approximation

Through the GKBA, the self-energy functional Σ^{\lessgtr} turn into functional of the retarded Green's function and one-particle density matrix, i.e., $\Sigma^{\lessgtr} [G^>, G^<] \rightarrow \Sigma^{\lessgtr} [G^R, \rho]$. Using the GKBA also in Eq. (66) the collision integral becomes:

$$\underline{I}(t) = - \int_{-\infty}^t dt' \mathcal{F} \left[\underline{\Sigma}^{\lessgtr}(t', t) \left[\underline{G}^R, \underline{\rho} \right], \underline{G}^R(t, t'), \underline{\rho}(t') \right] \quad (70)$$

i.e. $I(t)$ is an implicit functional, via Σ^{\lessgtr} , and also an explicit functional of the whole history of $\rho(t')$ for $t' < t$. The *Markovian approximation* (MA) consists in neglecting memory effects, thus evaluating Eq. (70) at the instantaneous density matrix $\rho(t)$:

$$\underline{I}^{\text{MA}}(t) = - \int_{-\infty}^t dt' \mathcal{F} \left[\underline{\Sigma}^{\lessgtr}(t', t) \left[\underline{G}^R, \underline{\rho}(t) \right], \underline{G}^R(t, t'), \underline{\rho}(t) \right]. \quad (71)$$

where now I^{MA} is a functional of the instantaneous density. The MA is justified provided that the electron dynamics is slow on the time-scale over which the self-energy decays.

If we further assume that the effects of a change in the density matrix on the quasi-particle Hamiltonian $h^{\text{qp}}(t)$ are only minor then we can use the equilibrium value h_0^{qp} (which is independent of time) to evaluate the propagator:

$$\underline{G}^{\text{R}}(t, t') = -i\theta(t - t') e^{-ih_0^{\text{qp}}(t-t')}. \quad (72)$$

Assuming $h_{ij}^{\text{qp}} = \delta_{ij}\epsilon_i^{\text{QP}}$ (see Section 4.1.1), the propagator gets the simpler expression

$$G_{ij}^{\text{R}}(t, t') = -i\delta_{ij}\theta(t - t')e^{-i\epsilon_i^{\text{QP}}(t-t')}. \quad (73)$$

With these approximations the time integral in $I(t)$ can be done analytically with the integrand depending only on the time difference $t - t'$:

$$\underline{I}^{\text{MA}}(t) \approx - \int_{-\infty}^t dt' \underline{\mathcal{K}}[\underline{\rho}(t)](t - t'). \quad (74)$$

Where the \mathcal{K} functional is constructed explicitly using Eq. (72) in the definition of the \mathcal{F} functional. The dependence on $t - t'$ stems from the time-translational invariance of G^{R} and it is therefore given by simple exponential functions.

5.4. Equilibrium self-energies taken out-of-equilibrium

All self-energies defined in Section 4.1.1 can be taken out-of-equilibrium by using NEGF techniques [53]. The procedure is to take all time arguments on the Keldysh contour and apply Langreth rules (see Chapter 5 of Ref.[53]).

The procedure is tedious but straightforward. In some cases, like the electronic GW approximation, the self-energy in the out-of-equilibrium regime acquires a different form compared to the equilibrium case.

In this section we illustrate the MA using the 2B self-energy, Eq. (41). The electronic and phononic GW self-energies written out-of-equilibrium by using the GKBA and MA can be found, for example, in Ref.[58, 59]. In this case the self-energy is an instantaneous functional of $\underline{G}^{\lessgtr}(t, t')$

$$\Sigma_{ij}^{\lessgtr}(t, t') = \sum_{nmpqsr} v_{irpn} w_{mqsj} G_{nm}^{\lessgtr}(t, t') G_{pq}^{\lessgtr}(t, t') G_{sr}^{\lessgtr}(t', t), \quad (75)$$

where

$$w_{imnj} \equiv v_{imnj} - v_{imjn}. \quad (76)$$

Using the GKBA expression for the lesser and greater Green's function and by replacing the pair $\rho(t')$ and $\bar{\rho}(t')$ with the pair $\rho(t)$ and $\bar{\rho}(t)$ the collision integral can be rewritten as

$$\begin{aligned}
I_{ik}^{\text{MA}}(t) &= \sum_{nmpqsr} \sum_j v_{irpn} w_{mqsj} \int_{-\infty}^t dt' \\
&\left[(G^{\text{R}}(t, t') \rho(t))_{nm} (G^{\text{R}}(t, t') \rho(t))_{pq} (\bar{\rho}(t) G^{\text{A}}(t', t))_{sr} (\bar{\rho}(t) G^{\text{A}}(t', t))_{jk} \right. \\
&\quad \left. - (G^{\text{R}}(t, t') \bar{\rho}(t))_{nm} (G^{\text{R}}(t, t') \bar{\rho}(t))_{pq} (\rho(t) G^{\text{A}}(t', t))_{sr} (\rho(t) G^{\text{A}}(t', t))_{jk} \right] \\
&= \sum_{nmpqsr} \sum_j v_{irpn} w_{mqsj} \left[\rho_{nm}(t) \rho_{pq}(t) \bar{\rho}_{sr}(t) \bar{\rho}_{jk}(t) - \bar{\rho}_{nm}(t) \bar{\rho}_{pq}(t) \rho_{sr}(t) \rho_{jk}(t) \right] \\
&\quad \times \int_{-\infty}^t dt' e^{-i(\epsilon_n^{\text{qp}} + \epsilon_p^{\text{qp}} - \epsilon_r^{\text{qp}} - \epsilon_k^{\text{qp}})(t-t')}. \quad (77)
\end{aligned}$$

From Eq. (77) it is evident that the collision integral is a quartic polynomial in $\rho(t)$. As anticipated, the integral over t' can be done analytically due to the simplicity of the propagator in Eq. (73). Thus the equation of motion for ρ reduces to a nonlinear differential equation with temporal scaling reduced from quadratic to linear, by maintaining the *same scaling with the system size*. It is worth noting that it has been recently shown that linear scaling in time can be achieved within GKBA without introducing further approximations, but at the cost of worsening the scaling with the system size [139, 140, 141].

6. Time-Resolved ARPES

In time-resolved and angle-resolved photo-emission (tr-ARPES) experiments on semiconductors or insulators a pump pulse excites electrons from the valence band to the conduction band. The photocurrent is generated by a *probe* pulse which impinges the system and causes the emission of electrons from the instantaneously filled states. Below we present an expression for the momentum resolved photocurrent in terms of the lesser Green's function of the solid. Here we assume that the system is translationally invariant with quasi momentum \mathbf{k} and therefore it is useful to re-expand explicitly the index i used so far as $i \rightarrow i\mathbf{k}\sigma$. In particular $\hat{c}_{i\mathbf{k}\sigma}^{(\dagger)}$ annihilates (creates) an electron of momentum \mathbf{k} with spin σ in band i and energy $\epsilon_{i\mathbf{k}}^{\text{qp}}$, and the corresponding lesser and

greater Green's function in Eq. 19 become

$$G_{ijk}^<(t, t') = i\langle \hat{c}_{jk\sigma}^\dagger(t') \hat{c}_{ik\sigma}(t) \rangle, \quad (78a)$$

$$G_{ijk}^>(t, t') = -i\langle \hat{c}_{ik\sigma}(t) \hat{c}_{jk\sigma}^\dagger(t') \rangle. \quad (78b)$$

Similarly we have that $\mu \rightarrow \mu\mathbf{q}$, with \mathbf{q} transferred momentum and

$$g_{ij}^\mu \Rightarrow g_{kij}^{\mathbf{q}\mu}, \quad (79a)$$

$$v_{ijml} \Rightarrow v_{ik\mathbf{k}}^{\mathbf{q}} \cdot \begin{matrix} \\ \\ mk\mathbf{p} \end{matrix}. \quad (79b)$$

In all above definitions we assumed for simplicity that the material is invariant under spin rotations. The generalization to non spin-compensated systems is straightforward. In the case where the pump and probe fields are overlapping in time explicitly gauge-invariant expressions for the photo-current have been proposed[142, 143]. Nevertheless, as explained in Section 3, in this work we assume to be in the dipole approximation. Therefore the full Hamiltonian in the presence of the pump field is itself gauge invariant as only the gauge-invariant electric field enters. Consequently, in the dipole approximation adopted here no extra terms has to be added to restore the gauge invariance.

The tr-ARPES signal is proportional to the number of electrons $N_{\mathbf{k}}(\omega)$ with energy ω and parallel momentum \mathbf{k} ejected by a probe pulse. For an arbitrary probe pulse of temporal profile $e(t)$ we have [144]

$$N_{\mathbf{k}}(\omega) = 2 \sum_{ij} \int dt dt' \operatorname{Re} \left[\Sigma_{ijk}^{\mathbf{R}}(\omega, t, t') G_{jik}^<(t', t) \right]. \quad (80)$$

The ionization self-energy reads [111]

$$\Sigma_{ijk}^{\mathbf{R}}(\omega, t, t') = -i\theta(t - t') d_{ik} e(t) e^{-i\omega(t-t')} d_{jk} e(t'), \quad (81)$$

where d_{ik} is the dipole matrix element between a state in band i and momentum \mathbf{k} and a continuum time-reversed LEED state of energy ω and parallel momentum \mathbf{k} . Eq. (80) is valid for systems in arbitrary non-equilibrium states and for any temporal shape and *intensity* of the probe field (hence even beyond linear response), the only approximation being that LEED electrons do not interact with bound electrons. A similar expression for $N_{\mathbf{k}}(\omega)$ was derived in Ref. [145]. We notice also that the photocurrent is a functional of

the probe pulse $e(t)$ and, therefore, it depends on the time T at which the pulse impinges the system. However, from Eq. (80) we see that $N_{\mathbf{k}}(\omega)$ is a complicated two-times convolution of $G^<$.

A simpler and more transparent expression can be obtained if the probe pulse has a duration t_p much longer than the typical electronic timescale and a frequency ω_p large enough to resolve the desired removal energies. In this case one can show that Eq. (80) reduces to [144, 51, 146, 147]

$$N_{\mathbf{k}}(\omega) \propto A_{\mathbf{k}}^<(T, \omega - \omega_p), \quad (82)$$

where T is the time at which the probe impinges the system and $A_{\mathbf{k}}^<$ is the transient (removal) spectral function

$$A_{\mathbf{k}}^<(T, \omega) = -i \int_{T+\frac{t_p}{2}}^{T-\frac{t_p}{2}} d\bar{t} e^{i\omega\bar{t}} \text{Tr} \left[G_{\mathbf{k}}^<\left(T + \frac{\bar{t}}{2}, T - \frac{\bar{t}}{2}\right) \right]. \quad (83)$$

In tr-ARPES experiments involving semiconductors with band-gap of the order of 1 eV, photo-excitation typically occurs via a NIR/VIS pump pulses. As a consequence we expect that the density matrix varies on a timescale of few femtoseconds, given by the inverse of the lowest excitation energy. Therefore the approximated expression in Eq. (83) can be safely used since typical probe fields are XUV pulses with duration t_p of some tens of femtoseconds.

6.1. Coherent and incoherent regimes: preliminary remarks

As the title of this review highlights we want to discuss the role played by coherence in the TR-ARPES phenomenology [148, 149, 150, 151, 152, 153]. As it was introduced in the Section 2 by using simple arguments, the excitation with an external laser pulse transfers coherence in the system. The most striking evidence of this coherence is the appearance of a finite polarization, which reflects the coherent oscillation of the system.

The finite polarization, however, is not the only fingerprint of a coherent dynamics. As it will be discussed in the following the microscopic properties of the system will be affected and the a consequent rich phenomenology appears.

Let's, however, come shortly back on the definition of the coherent regime by using the arguments used in Figure 1 of Ref.[54], that we reproduce here in Fig.5. After the

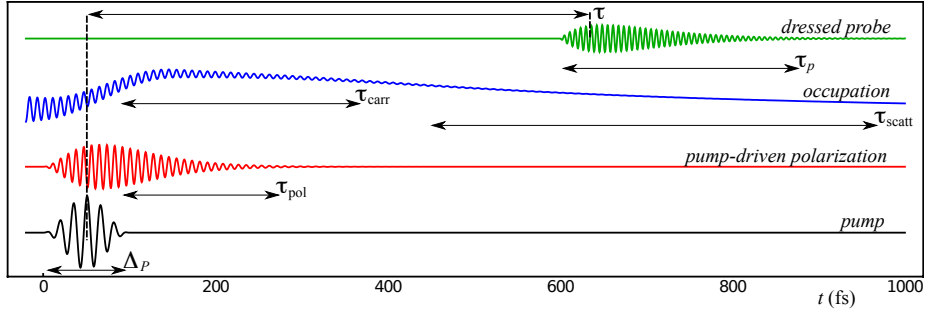


Figure 5: Illustration of the characteristic times occurring in a typical P&p experiment, from Ref.[54]. T_p is the time scale of the electron dynamics induced by the pump, θ_{pol} is the dephasing time of the pump-induced polarization, θ_{carr} is the stabilization time of the occupations, θ_{scatt} is the time to relax back to the equilibrium state, and θ_p is the lifetime of the dressed probe field. We also display the delay θ between pump and probe

pump field is applied it is well known that the system manifests a finite polarization that last for some time, θ_{pol} . Any experimentalist knows that this time scale depends on the specific system. In extended materials can be as long as ~ 100 fs, while in finite systems can be much longer.

While the pump pulse is active the quantum theory of elastic light scattering predicts the system to adsorb light at specific frequencies connected to the poles of the macroscopic dielectric function, Eq. (46). These frequencies can be obtained by solving the BSE, Eq. (51). This is commonly done in Material Science codes, like *Yambo* [154, 155] and for realistic materials it is found that the absorption frequencies can be located below the optical gap or above.

In the first case we talk of *excitons*, bound electron–hole pairs, whose energy lays in the single–particle forbidden region. When the absorption peak is located above the gap, instead, we talk of free electron–hole pairs. The physics of excitons is very rich and the microscopic properties of these exotic objects has been extensively studied. While a comprehensive review here is impossible we would like to mention the excitonic states, like the electronic states, suffer of scattering events. A paradigmatic example is the exciton–phonon scattering that in many works [156, 157, 158, 159, 160] has been proved to broaden the excitonic lines.

This broadening points to a internal structure of the excitonic states that reflect

their balance between the scatterings of the individual electrons/holes that participate to the excitonic state with the collective properties of the exciton as a new, bosonic like, particle. Actually the possibility to describe excitons as individual and well defined bosonic particles [161] is an highly debated aspect that already count for a long history of works [162, 163].

Going back to Fig.5 we see that the coherent regime lives as long as the polarization lives. After the decay of the polarization, also named *decoherence*, the system remains in an excited state where carriers are still populating the conduction bands. The question now is: are those carriers entirely embodied in excitonic states? Alternatively we could ask how the coherent picture evolves in the incoherent regime. As today there are no definitive answers to these questions. What we will review in the next sections is what we know on the coherent and incoherent regimes *with arguments firmly based on the NEGF approach*.

To this end we will consider two systems in the two regimes: (i) the two-bands model described by the H_{model}^{eq} , Eq. (17). (ii) a selection of realistic materials studied by means of *ab-initio* NEGF. We will consider bulk Silicon and Black-Phosphorus.

6.1.1. Excitonic signatures in the coherent regime of the model system

In the case of the Hamiltonian given by Eq. (17), the coherent regime, coincides with the *resonant pumping*, i.e. when the pump frequency ω_p matches the excitonic energy. In this case photo-excitation provides a direct and efficient excitation of excitons, since quasi-particle states are accessible only for $\omega_p > \epsilon_g$ [164, 165, 166, 167, 168, 169]. Indeed for H_{model}^{eq} there exist only one exciton, which can be made bound by tuning the Hamiltonian parameters, with energy ϵ_X .

We first characterize the many-body of the two-bands model as an oscillatory state that is generated by shining the system with a pump field with frequency $\omega_p = \epsilon_X$. We have recently shown [168, 51, 170] that after pumping the system is temporarily left in a BCS-like superfluid composed by a macroscopic number of excitons having a finite and oscillating polarization. Below we briefly discuss how to calculate the explicit wave-function of this superfluid since it is useful to predict the corresponding tr-ARPES spectrum.

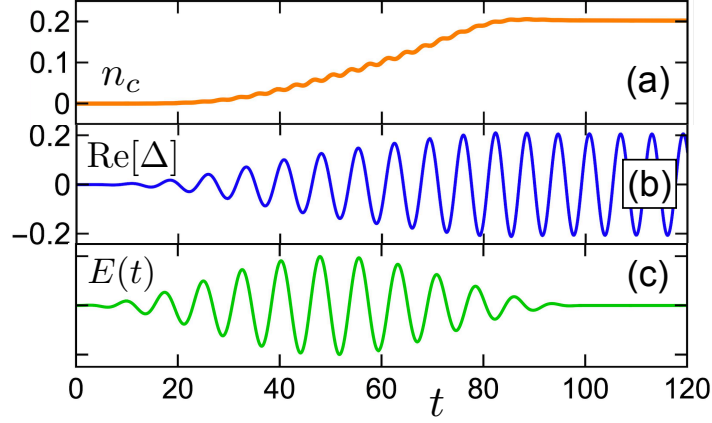


Figure 6: (a) Total density in the conduction band $n_c(t)$ and real part of the order parameter $\Delta(t)$ due to pumping with pump-profile shown in panel (c). We have considered the one-dimensional model in Eq. (17) with bandwidth $w = 2$, repulsion $U = 1$, constant dipole moments $D_k = D$, pumping intensity $\Omega_p = ED = 0.05$ (with E the pump amplitude) and pumping frequency $\omega_p \approx \epsilon_X = 0.76$. Energies are in units of the band-gap ϵ_g and times in units of $1/\epsilon_g$.

We further introduce a pumping term in the two bands model as

$$\hat{V}(t) = E(t) \sum_k D_k \left[\hat{c}_k^\dagger \hat{v}_k + \hat{v}_k^\dagger \hat{c}_k \right]. \quad (84)$$

Eq. (84) is added to H_{model}^{eq} to mimic the effect of Eq. (15) in Eq. (9). The numerical results (see Fig.6 and Ref.[168]) show that after pumping there is a finite and constant occupation of the conduction states $n_{ck} = \rho_{cck}$, and a finite residual polarization $\Delta(t) = -\frac{1}{\mathcal{L}} \sum_k \rho_{vck}(t)$ that exhibits persistent monochromatic oscillations at the excitonic frequency, i.e. $\Delta(t) = \Delta_0 e^{i\epsilon_X t}$.

The crucial point here is that the oscillatory density matrix $\rho(t)$ obtained from this simulation describes an excitonic superfluid, since it is *numerically identical* to the density matrix obtained by solving a static and self-consistent BCS-like problem [168]. The peculiarity of this mean-field problem consists in having different chemical potentials μ_c and μ_v for conduction and valence electrons, a pivotal feature to describe an excited

state. The secular equation reads

$$\begin{pmatrix} \epsilon_{vk} - \mu_v & U\Delta \\ U\Delta & \epsilon_{vk} - \mu_c \end{pmatrix} \begin{pmatrix} \varphi_{vk}^\xi \\ \varphi_{ck}^\xi \end{pmatrix} = \epsilon_k^\xi \begin{pmatrix} \varphi_{vk}^\xi \\ \varphi_{ck}^\xi \end{pmatrix}, \quad (85)$$

where $\xi = \pm$ labels the two eigensolutions, $\Delta = -\frac{1}{\mathcal{L}} \sum_k \varphi_{vk}^- \varphi_{ck}^-$ is the excitonic order parameter, and ϵ_k^ξ is the eigenvalue given by

$$\epsilon_k^\xi = \frac{\epsilon_{vk} + \epsilon_{ck} - \mu_v - \mu_c + \xi \sqrt{(\epsilon_{vk} - \epsilon_{ck} - \mu_v + \mu_c)^2 + 4U^2\Delta^2}}{2}. \quad (86)$$

If the difference between the chemical potentials is larger than the exciton energy ϵ_X , i.e., $\delta\mu = \mu_c - \mu_v > \epsilon_X$, the self-consistent problem in Eq.(85) admits a non-vanishing order parameter Δ , corresponding to an excitonic condensate solution [171, 166, 172, 173, 174, 175, 176, 177, 178, 168, 179, 180]. The superfluid is also characterized by a finite carrier density in conduction band

$$n_c = \frac{1}{\mathcal{L}} \sum_k |\varphi_{ck}^-|^2. \quad (87)$$

The dilute limit $n_c \ll 1$ of the solution is very interesting. In this case we have $\delta\mu \approx \epsilon_X$, and the order parameter Δ is very small. Thanks to these simplifications the self-consistent solution of Eq. (85) can be analytically determined. The lowest eigenvalue becomes $\epsilon_k^- = \epsilon_{vk} + \epsilon_X/2$, while the corresponding eigenvector φ_k^- can be written in terms of the excitonic eigenvector Y_k of the BSE equation (which the form that the BSE, Eq. (51) acquires for the two-bands model described by Eq. (17)):

$$(\epsilon_{ck} - \epsilon_{vk} - \epsilon_X) Y_k = \frac{U}{\mathcal{L}} \sum_q Y_q \quad (88)$$

as

$$\varphi_{vk}^- \approx 1, \quad (89a)$$

$$\varphi_{ck}^- \approx \sqrt{\mathcal{L}n_c} Y_k. \quad (89b)$$

Therefore the conduction component of the self-consistent solution is proportional to the exciton wave-function.

From the solution of Eq. (85) we can readily calculate the superfluid Green's functions. The Matsubara component $G_{ijk}^M(\tau, \tau^+) = i\varphi_{ik}^- \varphi_{jk}^- \equiv i\rho_{kij}^M$ can be used as initial

condition to extract the lesser component, having both arguments on the real axis:

$$G_{ijk}^<(t, t') = ie^{-i(\epsilon_k^- - \sigma_z \frac{\delta\mu}{2})t} \rho_k^M e^{i(\epsilon_k^- - \sigma_z \frac{\delta\mu}{2})t'}. \quad (90)$$

Notice that even if we have solved a static problem, $G^<(t, t')$ does *not* depend on the times difference. As a consequence the density matrix $\rho_k(t) = -iG_k^<(t, t)$ is not-stationary, since it has constant occupations, but time-dependent off-diagonal elements:

$$\rho_k(t) = \begin{pmatrix} |\varphi_{vk}^-|^2 & \varphi_{vk}^- \varphi_{ck}^- e^{i\delta\mu t} \\ \varphi_{vk}^- \varphi_{ck}^- e^{-i\delta\mu t} & |\varphi_{ck}^-|^2 \end{pmatrix} \equiv \begin{pmatrix} n_{vk} & \Delta_k e^{i\delta\mu t} \\ \Delta_k e^{-i\delta\mu t} & n_{ck} \end{pmatrix}. \quad (91)$$

As anticipated, our TD-HF simulations show that after weak resonant pumping the density matrix of the system is numerically identical to the one of Eq. (91), obtained with $\delta\mu = \epsilon_X$. This finding strongly suggests that an excitonic superfluid can be transiently created in real time by pumping a normal insulator in resonance with a bright exciton. Here the self-sustained oscillations generate a Floquet-like regime in the absence of external driving [171, 181, 168], and are expected to survive over a timescale dictated by the polarization lifetime. We mention that a particularly interesting instance may occur in systems with optically bright p -wave excitons. In this case it has been recently shown that resonant pumping could induce the creation of an exciton superfluid with nontrivial topological properties [147].

We have now all the ingredients to calculate the time-dependent photo-emission spectrum originating from the exciton superfluid. By substituting the expression for $G^<(t, t')$ in Eq. (90) in the formula (80) for the photocurrent, one can show that $N_k(\omega)$ takes the elegant and compact form [51]

$$N_k(\omega) = \left| \varphi_k^{-\dagger} \tilde{e} \left(\epsilon_k^- \hat{1} - \sigma_x \frac{\delta\mu}{2} - \omega \hat{1} \right) d_k \right|^2, \quad (92)$$

where $\tilde{e}(\omega)$ is the Fourier transform of the probe pulse $e(t)$.

It is instructive to further manipulate the above expression for low excited densities in two opposite cases, namely in the limit of a long-monochromatic probe, and in the limit of ultrashort probe. For $e(t) = e \sin[\omega_p(t - T)]$ (T being the time at which the probe impinges the system) we have

$$N_k(\omega) \propto \delta(\omega - \epsilon_v - \omega_p) + \mathcal{L}n_c |Y_k|^2 \delta(\omega - \epsilon_v - \epsilon_X - \omega_p). \quad (93)$$

The numerical evaluation of the above equation, for the same model parameters used in Fig.6 is shown in Fig.7(a). We clearly observe the occurrence of a quasi-particle peak at $\omega = \epsilon_{vk}$ corresponding to the removal an electron from the valence band, accompanied by an *excitonic satellite* inside the gap, at $\omega = \epsilon_{vk} + \epsilon_X$. The latter corresponds to the removal of an electron from the excitonic superfluid. As a function of the momentum, the exciton structure forms a side-band which is a replica of the valence band, shifted upward by ϵ_X [168, 51]. The spectral weight of the side-band is proportional to the carrier density n_c , and to the square modulus of the exciton wave-function $|Y_k|^2$. We also observe that in this case the photocurrent is essentially independent on the pump-probe delay T .

A comment on the physical origin of the excitonic side-band is in order. In the coherent regime the density matrix has off-diagonal elements that oscillate at frequency $\delta\mu$, see Eq.(91). Thus one can show that gran-canonical HF Hamiltonian in Eq (85) coincides with the Floquet Hamiltonian of the same system, subject to monochromatic driving with frequency $\delta\mu = \epsilon_X$. According to the Floquet theory, a replica of the originally filled band shifted upward by the driving frequency is expected to occur in the spectral function of the system [54].

We have shown that the above approach can be also implemented in ab-initio simulations of realistic materials. To this end we have considered LiF bulk [168], an insulator with band-gap $\epsilon_g = 14.5$ eV and having a 1s bright exciton with a binding energy $\epsilon_X = 12.5$ eV, and by using the *Yambo* [154, 155]code we have solved a first-principle version of the self-consistent problem in Eq. (85). Also in this case we have found a superfluid solution for $\delta\mu \gtrsim \epsilon_X$, giving rise to a photocurrent spectrum with an excitonic replica of the valence band appearing inside the gap.

The situation is completely different in the opposite limit of ultrashort probes. For $e(t) = e\delta(t - T)$ Eq. (92) yields

$$N_k(\omega) \propto C_k + Y_k \cos(\epsilon_X T + \phi_k), \quad (94)$$

where C_k is a ω -independent background and ϕ_k is a phase that depends on the dipole matrix elements d_k and on the probe amplitude e . In this limit $N_k(\omega)$ is independent on ω and has nothing to do with the original band-structure of the system. The pho-

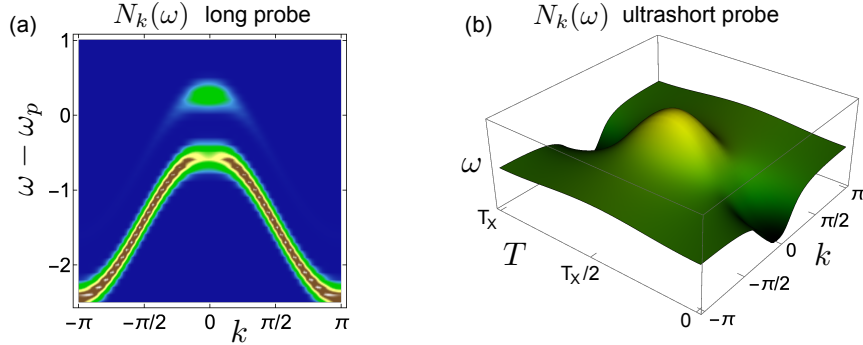


Figure 7: Transient photocurrent $N_k(\omega)$ for the one-dimensional system in Eq. (17) for the same parameters as in Fig.6 for monochromatic (panel a) and ultrashort (panel b) probe. Frequencies ω are measured with respect to the valence band maximum. Energies are in units of the band-gap ϵ_g and times in units of $1/\epsilon_g$.

tocurrent and is an oscillating function of the delay T , with period $T_X = 2\pi/\epsilon_X$ dictated by the exciton energy, see Fig.7(b). The oscillatory term is proportional to the exciton wave-function Y_k . Thus it appears that tr-ARPES experiments in the coherent regime with long or ultrashort probes can be used for a direct measurement of the exciton wave-function. This has been very recently demonstrated in tr-ARPES experiments on transition metal dichalcogenides employing probes with T_p of several tens of femtoseconds [182, 183].

In order to study the intermediate regime of finite-duration probes, we have to resume Eq. (92). In Fig.8 we display the transient photocurrent for a sinusoidal probe of duration T_p comparable with the excitonic period T_X . We see that $N_k(\omega)$ exhibits different features depending on the delay T . For small delays $T = 0$, the tr-ARPES spectrum resembles the simple valence band. For $T = T_X/4$ excitonic effects start to be visible, as there is a sizable transfer of spectral weight from the top of the valence band maximum toward higher energies. For $T = T_X/2$, the probe impinges the system when the real part of the order parameter is maximum, and the exciton satellite is fully developed inside the gap.

We conclude this section by commenting on the robustness of the predictions made in this section. The excitonic superfluid responsible for the peculiar spectral features discussed above is characterized by a *finite* excited density n_c . In principle excited

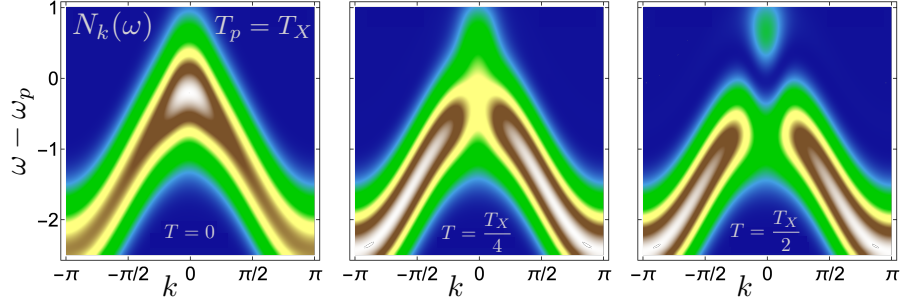


Figure 8: Transient photocurrent $N_k(\omega)$ for the one-dimensional system in Eq. (17) for the same parameters as in Fig.6 for a sinusoidal probe of frequency $\omega_p = 40$, duration $T_p = T_X \approx 8$ for three different delays $T \approx 0$, $T = T_X/4$, $T = T_X/2$. Frequencies ω are measured with respect to the valence band maximum. Energies are in units of the band-gap ϵ_g and times in units of $1/\epsilon_g$.

carriers could screen the Coulomb attraction, thus causing the disappearance of the superfluid phase. However, in a recent paper we have shown [51] that as long as the system hosts a finite order parameter, the long-wave component of the dielectric function vanishes. Indeed excitons are neutral composite quasi-particles with very scarce screening efficiency: a gas of microscopic electric dipoles is not capable to modify the long-distance behavior of the Coulomb repulsion. This remarkable property renders the exciton condensate particularly robust, at least for small and moderate excited density.

6.2. Incoherent regime: excitons versus quasiparticles

As discussed in Section 6.1 the incoherent regime appears when the induced polarization is dead and there are still carriers populating the conduction bands.

At long times (of the order of tens of picoseconds) after pumping, it is well known that incoherent effects caused by carrier-carrier [184, 185] and carrier-phonon [46, 138] scattering drive the system towards a relaxed and dephased regime where electrons (holes) remain trapped in the conduction (valence) band and place around the conduction band minimum (valence band maximum).

If we consider systems characterized by a sizable electron-hole attraction it is clear, from simple arguments, that the excited carriers will form bound states. At the same time it is natural to expect that these bound states will coexist with the plasma of free

carriers in an excited, quasi-stationary state whose description is a real challenge for theoreticians [186, 43, 144, 187].

In the following two sections we will tackle the problem from two very different perspectives: again using the two-bands model, Eq. (17), to demonstrate how the theory can capture the binding of the electron-hole photo-excited pairs; and the carriers perspective where we describe, using *ab-initio* methods the carrier dynamics in realistic materials and directly comparing to the experimental results.

6.2.1. Incoherent excitonic contribution in the model system

We consider again the two-bands model, Eq. (17), and we start observing that in this incoherent regime $G^<$ is diagonal in the band-index and depends only on the times-difference

$$G_{ij\mathbf{k}}^<(t, t') \approx \delta_{ij} G_{ii\mathbf{k}}^<(t - t'). \quad (95)$$

Therefore the transient spectral function in Eq. (83) is weakly dependent on the time T at which the probe arrives, and can be approximated as

$$A_{\mathbf{k}}^<(T, \omega) \approx A_{\mathbf{k}}^<(\omega) \approx -i \sum_i G_{ii\mathbf{k}}^<(\omega). \quad (96)$$

In addition, experiments [18, 16, 19, 56] and numerical simulations [188, 189], indicate that the electron occupations in the quasi-stationary excited state follow a Fermi-Dirac distribution with temperatures T_i and chemical potentials μ_i depending on the band index i . Clearly both T_i and μ_i vary on a picosecond time-scale but they can be considered as constant on the time-scale of the probe pulse. From such experimental and numerical evidence we infer that the recombination of electrons with different band index is severely suppressed and hence the lesser Green's function fulfills the approximate fluctuation-dissipation relation

$$G_{ii\mathbf{k}}^<(\omega) = -f_i(\omega) [G_{ii\mathbf{k}}^R(\omega) - G_{ii\mathbf{k}}^A(\omega)], \quad (97)$$

where $f_i(\omega) = 1/(e^{(\omega - \mu_i)/T_i} + 1)$ is the Fermi function for the band i . The i -dependent temperature and chemical potential can be extracted by a best fitting of the electronic populations as obtained from, e.g., the one-time GKBA propagation as it has been

shown in Ref. [188]. From Eq. (97) it appears that we are left with the evaluation of the retarded Green's function

$$G_{ii\mathbf{k}}^{\text{R}}(\omega) = \left[\frac{1}{\omega - h_{\mathbf{k}}^{\text{qp}} - \Sigma_{\mathbf{k}}^{\text{R}}(\omega)} \right]_{ii}, \quad (98)$$

where the T -matrix self-energy $\Sigma_{\mathbf{k}}^{\text{R}}$ carries all the information about the excitonic spectral features.

We now assume that the system is in a quasi-stationary excited state with a finite population in the conduction band, and show how to construct explicitly the T -matrix self-energy accounting for exciton signatures in the spectral function. We focus on the ARPES signal belonging to conduction electrons, and therefore in Eq. (96) we evaluate only the contribution $A_{cck}(\omega) \equiv -iG_{cck}^<(\omega)$. To this end we need the conduction-conduction self-energy $\Sigma_{ccp}(\omega)$.

In the relaxed excited state, let $f_{ip} = \rho_{iip}$ be the population of the state in band $i = v, c$ with momentum p . Accordingly, the undressed quasi-particle Green's functions in the HF approximation read

$$g_{ip}^<(\omega) = 2\pi i f_{ip} \delta(\omega - \epsilon_{ip}), \quad (99a)$$

$$g_{ip}^>(\omega) = -2\pi i \bar{f}_{ip} \delta(\omega - \epsilon_{ip}), \quad (99b)$$

with $\bar{f}_{ip} = 1 - f_{ip}$. Using these quasi-stationary Green's function to calculate the lesser/greater T -matrix self-energy we find

$$\Sigma_{ccp}^<(\omega) = iU^2 \sum_q f_{vp-q} L^{q,<}(\omega - \epsilon_{vp-q}), \quad (100a)$$

$$\Sigma_{ccp}^>(\omega) = -iU^2 \sum_q \bar{f}_{vp-q} L^{q,>}(\omega - \epsilon_{vp-q}), \quad (100b)$$

where L^{\lessgtr} are the lesser/greater components of the dresses electron-hole propagator. They are related to the retarded and advanced components $L^{\text{R/A}}$ via the relations [50]

$$L^{q,<} = -2\eta \sum_{kk'p} L_{kp}^{q,\text{R}}(\omega) \frac{f_{cp+q} \bar{f}_{vp}}{(f_{vp} - f_{cp+q})^2} L_{pk'}^{q,\text{A}}(\omega), \quad (101a)$$

$$L^{q,>} = -2\eta \sum_{kk'p} L_{kp}^{q,\text{R}}(\omega) \frac{\bar{f}_{cp+q} f_{vp}}{(f_{vp} - f_{cp+q})^2} L_{pk'}^{q,\text{A}}(\omega). \quad (101b)$$

The equations close as the retarded electron-hole propagator satisfies the BSE, Eq. (51)

$$L_{kk'}^{q,R}(\omega) = L_{0,kk'}^{q,R}(\omega) + \frac{i}{\mathcal{L}} \sum_p L_{0,kp}^{q,R} U L_{pk'}^{q,R}(\omega) \quad (102)$$

where non-interacting propagator is evaluated with the undressed Green's functions in Eq. (99) and is given by

$$L_{0,kk'}^{q,R}(\omega) = i\delta_{kk'} \frac{f_{vk} - f_{ck+q}}{\omega - \epsilon_{ck+q} + \epsilon_{vk} + i\eta}. \quad (103)$$

Having the lesser/greater self-energy we can calculate Σ_{cc}^R from the Hilbert transform of $\Sigma_{cc}^> - \Sigma_{cc}^<$. The retarded Green's function therefore is calculated as

$$G_{cck}^{(R)}(\omega) = \frac{1}{\omega - \epsilon_{ck} - \Sigma_{cck}^R(\omega)}, \quad (104)$$

and according to Eq. (97), the desired conduction spectral function is

$$A_{cck}(\omega) = -2f_c(\omega)\text{Im}[G_{cck}^{(R)}(\omega)]. \quad (105)$$

We observe that the vertex correction in the self-energy carried by the electron-hole correlator L is crucial to produce the excitonic satellite in the spectral function. Indeed the non-perturbative summation in the BSE, Eq. (102), generates the exciton peak in $L^{q,R}(\omega)$, occurring at energy $\epsilon_X = \epsilon_{c0} - \epsilon_{v0} - b_X$, i.e. *below* the onset of the particle-hole continuum. The presence of such split-off structure is then transmitted to the self-energy via Eq. (100).

Explicit calculations have been performed by considering a model dispersion $\epsilon_{vk} = (w/2)\cos k$ and $\epsilon_{ck} = -(w/2)\cos k + w + \epsilon_g$, with bandwidth $w = 4$ eV, band-gap $\epsilon_g = 1$ eV, and repulsion $U = 2$ eV. With these parameters the conduction band minimum occurs at $\epsilon_{c0} = 3$ eV, and there is an exciton state with binding energy $b_X \approx 0.42$ eV. The excited distribution functions are taken at temperatures $T = T_v = T_c = 4000$ K with $\mu_v = 2.35$ eV and $\mu_c = 2.65$ eV. In Fig. 9 (left panel) we show $A_{cc0}(\omega)$ for different carrier densities $n_c = \frac{1}{\mathcal{L}} \sum_k f_{ck}$. At very low density $n_c \lesssim 10^{-4}$ the system is essentially in equilibrium and the photocurrent is vanishingly small (not shown). At density $n_c \approx 10^{-3}$ a quasi-particle peak at $\omega \approx 3$ eV appears. This corresponds to the removal energy of an excited electron from the bottom of the conduction band. As the

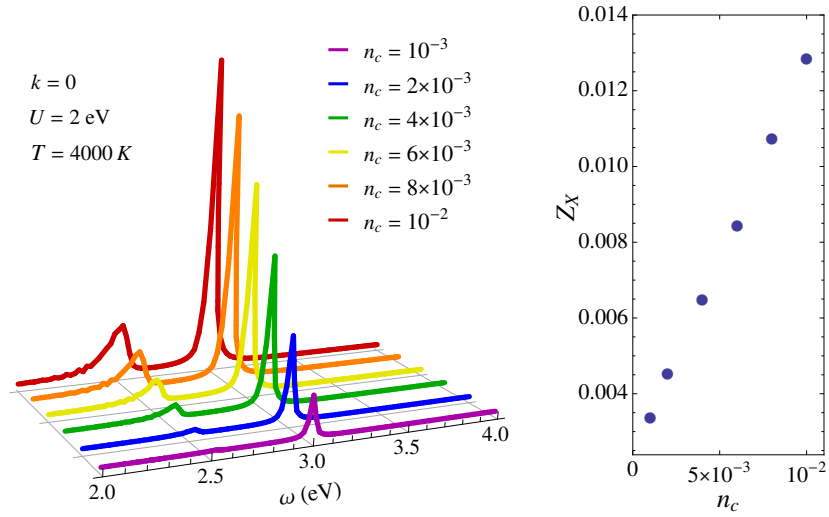


Figure 9: Left panel: Spectral function $A_{cc,0}(\omega)$ (in arbitrary units) for different densities of the conduction electrons n_c at temperature $T = 4000$ K. Right panel: Dependence of the exciton weight Z_X on n_c . The convergence parameters are $\eta = \omega/(4\mathcal{L})$ and $\mathcal{L} = 80$.

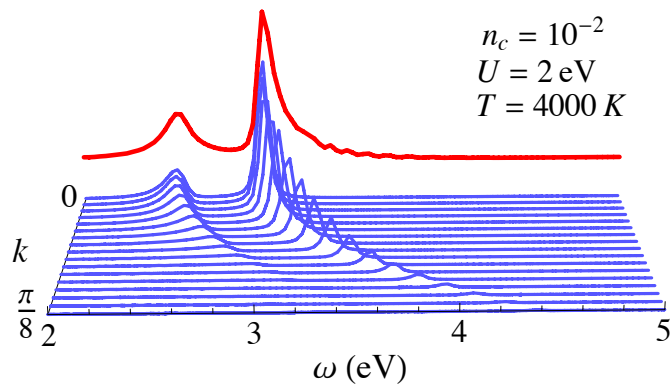


Figure 10: Spectral function $A_{cc,k}(\omega)$ (in arbitrary units) for different momenta k . The (red) curve in the background is the integrated quantity $\int dk A_{cc,k}(\omega)$. Same parameters as in Fig. 9 and $n_c = 10^{-2}$.

density increases, a satellite appears inside the gap, at energy $\epsilon_{c0} - b_X \approx 2.5$ eV. This is clearly the exciton fingerprint discussed above. We can also calculate the spectral function for different momenta k of the conduction electron. This quantity is relevant to address angle-resolved experiments. In Fig. 10 we plot $A_{cck}(\omega)$ in the range $0 < k < \pi/8$. We observe that the angle-resolved photocurrent displays an *excitonic sideband* inside the gap, which is almost parallel to the conduction band. Similar results have been recently found by other authors by using an analogous T -matrix approach to describe highly excited transition metal dichalcogenides [187].

6.2.2. Coherent excitation and incoherent carriers migration

A crucial result of the previous section is the possibility, in the model, to calculate the excitonic weight

$$Z_X = - \int_{-\infty}^{\epsilon_{c0}} \frac{d\omega}{2\pi} \text{Im} \left[G_{cc,0}^R(\omega) \right]. \quad (106)$$

It has been pointed out that this quantity provides an estimate of the number of incoherent excitons coexisting with the plasma of free carriers in conduction band [187]. From the right panel of Fig. 9 we see that Z_X increases with the density following a linear trend. From this analysis is evident that free carriers and bound states will coexist and, as it is numerically still unfeasible to take into account, within an *ab-initio* scheme, excitons in the out-of-equilibrium dynamics the question is to what extent a purely carriers description is adequate?

Most of the methods currently used in the Material Science community are not based on formal justification, as it is not possible to derive analytical solution for realistic materials. The methods are based on a Test & Validate scheme. Approximations, like DFT-LDA, are applied on a many materials and the practical justification of the approach is revealed from the success in describing the experimental results. In practice also the GW/BSE scheme has been devised in this way [75].

In order to formally move from the excitonic picture (introduced in the model) to the carriers representation we start by approximating the transient spectral function in Eq. (83). We assume that the system is instantaneously in a *quasi-equilibrium* state characterized by well-defined quasiparticles and by a vanishing polarization. Under this

adiabatic condition, we can use the GKBA to express the quasi-particle $G^<$ in Eq. (83) as

$$\begin{aligned} G_{\mathbf{k}ij}^< \left(T + \frac{\bar{t}}{2}, T - \frac{\bar{t}}{2} \right) &\approx \\ &- \delta_{ij} \rho_{\mathbf{k}ii}(T) \left[G_{\mathbf{k}ii}^R \left(T + \frac{\bar{t}}{2}, T - \frac{\bar{t}}{2} \right) - G_{\mathbf{k}ii}^A \left(T + \frac{\bar{t}}{2}, T - \frac{\bar{t}}{2} \right) \right] \\ &\approx -\delta_{ij} \rho_{\mathbf{k}ii}(T) \left[G_{\mathbf{k}ii}^R(\bar{t}) - G_{\mathbf{k}ii}^A(\bar{t}) \right], \end{aligned} \quad (107)$$

where in the last line we have used the quasi-equilibrium assumption that $G^{R/A}$ depends only on the time difference \bar{t} . Therefore for long-probe duration t_p the transient spectral function becomes

$$A_{\mathbf{k}}^<(T, \omega) \approx i \sum_i \rho_{\mathbf{k}ii}(T) \left[G_{\mathbf{k}ii}^R(\omega) - G_{\mathbf{k}ii}^A(\omega) \right], \quad (108)$$

where

$$G_{\mathbf{k}ii}^{R/A}(\omega) = \left[\frac{1}{\omega - \epsilon_{\mathbf{k}}^{\text{qp}} \pm i\eta} \right]_{ii} \approx \frac{1}{\omega - \epsilon_{i\mathbf{k}}^{\text{qp}} \pm i\eta}. \quad (109)$$

We thus arrive at the result that the tr-ARPES spectrum is proportional to the sum of the equilibrium spectral functions of the different bands i , weighted by the corresponding time-evolving occupations $f_{\mathbf{k}i}(T) = \rho_{\mathbf{k}ii}(T)$.

If this approach does not allow to introduce incoherent excitonic effects in sense of Section 6.2.1 it allows to introduce de-coherence effects in the form of electron–electron and electron–phonon scattering. These processes, as it will clear shortly, are essential to quantitatively capture the physics observed experimentally in realistic materials.

The scheme that we will describe in the following is currently implemented in the *Yambo* [154, 155] code and it has been applied on a wealth of systems and observable: it has been applied to 2D Semiconductors to calculate transient absorption[190, 191, 137], Kerr angle[192, 138], TR-ARPES [193, 57].

In *Yambo* the out-of-equilibrium dynamics is split in two parts: the coherent excitation and the carriers scattering. In practice this means that the KBE, Eq. (61), is reduced, by using the GKBA and the MA [58, 59] to a non-linear differential equation for $\rho_{\mathbf{k}ii}(T)$:

$$\frac{\partial}{\partial T} f_{\mathbf{k}i}(T) = \frac{\partial}{\partial T} f_{\mathbf{k}i}(T) \Big|_{coh} + \frac{\partial}{\partial T} f_{\mathbf{k}i}(T) \Big|_{scatt}, \quad (110)$$

with the scattering term composed of an electron–electron and electron–phonon contribution:

$$\left. \frac{\partial}{\partial T} f_{\mathbf{k}i}(T) \right|_{scatt} = \left. \frac{\partial}{\partial T} f_{\mathbf{k}i}(T) \right|_{scatt}^{e-e} + \left. \frac{\partial}{\partial T} f_{\mathbf{k}i}(T) \right|_{scatt}^{e-p}. \quad (111)$$

The coherent excitation. The coherent term in Eq. (110), as encoded in *Yambo*, fully takes into account excitonic effects. In practice this means that Eq. (50) is used with the HF self–energy replaced by the statically screened *GW* self–energy (SEX approximation). More details can be found in Ref.[194]. In practice we have that

$$\left. \frac{\partial}{\partial T} \rho_{\mathbf{k}}(T) \right|_{coh} = - \left[\underline{h}_{\mathbf{k}}^{KS} + \underline{\delta V}_{\mathbf{k}}^{Hartree}(T) + \underline{\delta \Sigma}_{\mathbf{k}}^{SEX}(T) + \underline{V}_{\mathbf{k}}(T), \rho_{\mathbf{k}}(T) \right], \quad (112)$$

with $\delta V^{Hartree}$ and $\delta \Sigma^{SEX}$ the variations with respect to equilibrium of the Hartree and SEX self–energies. Eq. (112) gives is exactly equivalent to the static BSE commonly applied in modern *ab–initio* codes[75]. The coherent scattering term in Eq. (110) ensures that the excitation process correctly capture excitonic effects and quantitatively reproduces the experimental excitation process.

The scattering processes are embodied in the second term of Eq. (110) and are the result of the application of the Markovian approximation, Section 5.3, and GKBA, Section 5.2, to the *GW* self–energies described in Section 5.4. The resulting e–e and e–p scattering terms are:

$$\begin{aligned} \left. \frac{\partial}{\partial T} f_{\mathbf{k}i}(T) \right|_{scatt}^{e-p} &= -\gamma_{\mathbf{k}i}^{(e-p, \nearrow)}(T) f_{\mathbf{k}i}(T) + \bar{\gamma}_{\mathbf{k}i}^{(e-p, \nearrow)}(T) \bar{f}_{\mathbf{k}i}(T) \\ &\quad - \gamma_{\mathbf{k}i}^{(e-p, \searrow)}(T) f_{\mathbf{k}i}(T) + \bar{\gamma}_{\mathbf{k}i}^{(e-p, \searrow)}(T) \bar{f}_{\mathbf{k}i}(T) \end{aligned} \quad (113)$$

In Eq. (113) the $\gamma_{\mathbf{k}i}^{(e-p, \nearrow)}$ are the NEQ carrier lifetimes which describes the scattering of carriers from one level and momenta to another by absorbing(\searrow)/emitting(\nearrow) a phonon.

$$\gamma_{\mathbf{k}i}^{(e-p, \nearrow)}(T) = \pi \sum_{j\mathbf{q}\mu} \frac{|g_{\mathbf{k}ij}^{\mathbf{q}\mu}|^2}{N_{\mathbf{q}}} \delta(\epsilon_{\mathbf{k}-\mathbf{q}j} - \epsilon_{\mathbf{k}i} \pm \omega_{\mathbf{q}\mu}) \begin{pmatrix} 1 + f_{Bose}^{\mathbf{q}\mu}(T) \\ f_{Bose}^{\mathbf{q}\mu}(T) \end{pmatrix} \bar{f}_{\mathbf{k}-\mathbf{q}j}(T), \quad (114a)$$

$$\bar{\gamma}_{\mathbf{k}i}^{(e-p, \searrow)}(T) = \sum_{j\mathbf{q}\mu} \frac{|g_{\mathbf{k}ij}^{\mathbf{q}\mu}|^2}{N_{\mathbf{q}}} \delta(\epsilon_{\mathbf{k}-\mathbf{q}j} - \epsilon_{\mathbf{k}i} \pm \omega_{\mathbf{q}\mu}) \begin{pmatrix} f_{Bose}^{\mathbf{q}\mu}(T) \\ 1 + f_{Bose}^{\mathbf{q}\mu}(T) \end{pmatrix} f_{\mathbf{k}-\mathbf{q}j}(T). \quad (114b)$$

In Eq. (113) and Eq. (114) we have labeled the hole counterparts of the occupations and line-widths as $\bar{f} = 2 - f$ and $\bar{\gamma}$. Moreover $f_{Bose}^{\mathbf{q}\mu}(T)$ is the occupation of the phonon mode $\mathbf{q}\mu$ at temperature T . Thus Eq. (114) naturally embody the temperature dependence.

A similar derivation can be done for the e-e channel [58, 59]:

$$\frac{\partial}{\partial T} f_{\mathbf{k}i}(T) \Big|_{scatt}^{e-e} = \gamma_{\mathbf{k}i}^{(e-e)}(T) f_{\mathbf{k}i}(T) - \bar{\gamma}_{\mathbf{k}i}^{(e-e)}(T) \bar{f}_{\mathbf{k}i}(T), \quad (115)$$

with

$$\begin{aligned} \gamma_{\mathbf{k}i}^{(e-e)}(T) &= \frac{4\pi}{N_{\mathbf{q}}\Omega} \sum_{\mathbf{q}\mathbf{p}} \sum_{jlm} \left| W_{ij\mathbf{k}}^{\mathbf{q}} \right|_{ml\mathbf{p}}^2 \\ &\delta(\epsilon_{\mathbf{k}-\mathbf{q}j} + \epsilon_{\mathbf{p}m} - \epsilon_{\mathbf{p}-\mathbf{q}l} - \epsilon_{\mathbf{k}i}) \bar{f}_{\mathbf{k}-\mathbf{q}j}(T) \bar{f}_{\mathbf{p}m}(T) f_{\mathbf{p}-\mathbf{q}l}(T), \end{aligned} \quad (116a)$$

and

$$\begin{aligned} \bar{\gamma}_{\mathbf{k}i}^{(e-e)}(T) &= \frac{4\pi}{N_{\mathbf{q}}\Omega} \sum_{\mathbf{q}\mathbf{p}} \sum_{jlm} \left| W_{ij\mathbf{k}}^{\mathbf{q}} \right|_{ml\mathbf{p}}^2 \\ &\delta(\epsilon_{\mathbf{k}-\mathbf{q}j} + \epsilon_{\mathbf{p}m} - \epsilon_{\mathbf{p}-\mathbf{q}l} - \epsilon_{\mathbf{k}i}) f_{\mathbf{k}-\mathbf{q}j}(T) f_{\mathbf{p}m}(T) \bar{f}_{\mathbf{p}-\mathbf{q}l}(T), \end{aligned} \quad (116b)$$

Eq. (114) and Eq. (116) describes a simple $(\mathbf{k}i) \rightarrow (\mathbf{k} - \mathbf{q})$ mediated by phonons and electron-hole pairs. The scatterings can have different kinematic geometries and few of them are schematically discussed in Fig.11. In the left frame an electron excited in the conduction bands, in the state i scatters to an higher state, j by absorbing a phonon $\omega_{\mathbf{q}\mu}$. In the same frame a hole in the state i is filled by an electron from state j by emitting a phonon. These two processes alter the phonon population.

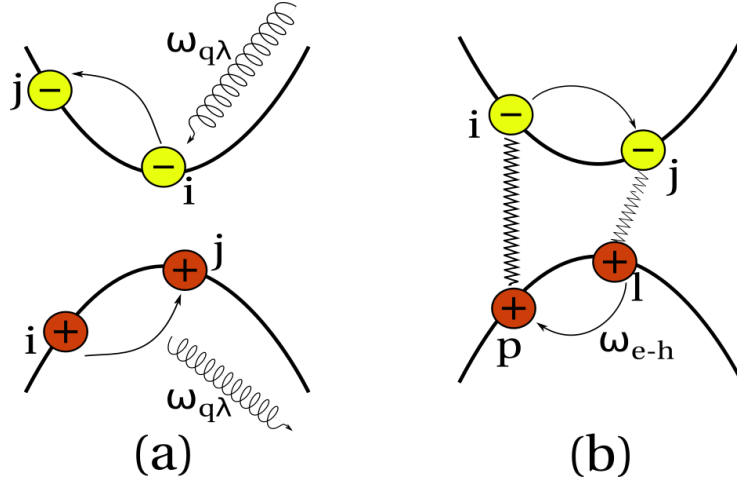


Figure 11: Schematic representation of the elemental carrier scattering processes mediated by phonons and electron–hole pairs. From Ref. [59]. The process (a) represents the physics of $\gamma_{\mathbf{k}i}^{(e-p,\lambda)}(T)$ in the conduction and $\bar{\gamma}_{\mathbf{k}i}^{(e-p,\lambda)}(T)$ in the valence, Eq. (113). In the (b) case, instead, the scattering $(\mathbf{k}i) \rightarrow (\mathbf{k} - \mathbf{q})$ is energetically compensated by the promotion of an electron in the valence. This is $\gamma_{\mathbf{k}i}^{(e-e)}(T)$, from Eq. (116).

Similarly, in the right frame of Fig.11, the electron i moves to a lower state, j by releasing the energy which is used to promote the electron in the p state to the final, higher, l state.

6.3. Time-Resolved ARPES from first-principles in two paradigmatic materials: bulk Silicon and Black-Phosphorus

Eq. (110) has been applied in several materials and to describe a wealth of time-dependent physical observable. The specific case of the TR-ARPES was the subject of Ref.[193] and Ref.[57] where two paradigmatic materials are investigated: bulk Silicon and bulk Black-Phosphorus.

6.3.1. Symmetry breaking and ultra-fast restoring in Bulk Silicon

Bulk Silicon is a paradigmatic material from different point of views. It is an indirect semiconductor with moderate excitonic effects [195]. The fact that is indirect makes it impossible to model with simple parametric Hamiltonians, like H_{model}^{eq} . At the same time it has been extensively used as a test-bed for several theories and phenomena [56,

196, 197, 198, 199, 200, 201]. In Ref.[55] a *Si* wafer, oriented both along the [111] and the [100] surface directions, is excited with a laser pulse at room temperature. The photo-excited sample is, then, probed with a second laser pulse that photo-emits in the continuum the excited carriers. The photo-emitted current of electrons is measured as a function of the time delay between the pump and the probe. The final result is a measure of the time-dependent occupation of the valence bands (represented by the dots in the main frame of Fig.12). More specifically the population of carriers near the point L_1 , i.e. at $E \approx 1.6$ eV above the Fermi level is probed.

The agreement between theory and experiment is excellent. Both the gradual filling and emptying of the L_1 state follows quite nicely the experimental curve. The theoretical results correctly describe the ultra-fast decay time-scale (~ 180 fs) and the 40 fs shift of the population peak from the maximum of the pump pulse. The 40 fs delay reflects the delicate balance between the photo-excitation and the e-p scattering and can only be described by treating both processes on the same footing.

Experimentally [55] the ultra-fast decay of the L_1 state is interpreted as due to $L_1 \rightarrow X_1$ transitions. However a more deep analysis of the theoretical result reveals a very different scenario.

In Fig.12(a), the population of the levels at $t = 0$ is shown. Blue lines represent charges added and red lines charges removed. The band structure is computed along the $L\Gamma L'$ high symmetry path in the Brillouin Zone (BZ). In bulk *Si* L and L' are equivalent points but Fig.12.a shows that the level L'_1 is not populated and most of the carriers are injected in the L_1 level.

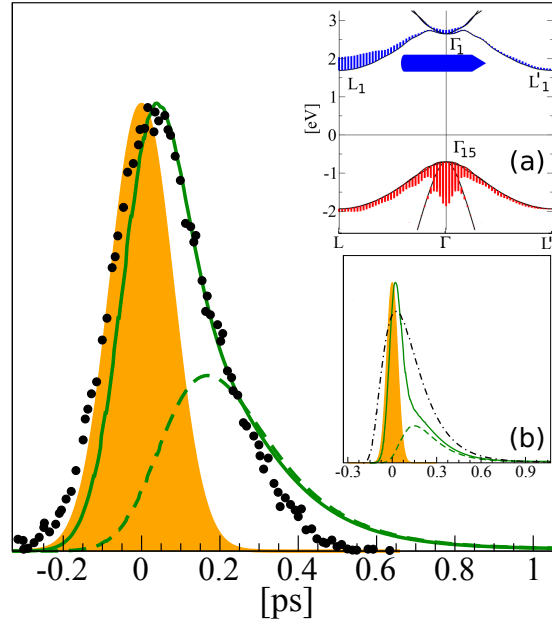


Figure 12: The time dependent occupation of the L_1 (green continuous line) and L'_1 (green dashed line) levels are compared with experimental data (black dots) from Ref.[55]. The envelope of the laser pulse is also represented (orange shadow). In the inset (a) the carriers population (electrons in blue, holes in red) is super imposed on the band-structure at $t = 0$. The blue arrow indicates the direction of the ultra-fast $L_1 \rightarrow L'_1$ scattering process. In the inset (b) the dynamics with a shorter laser pulse ($\sigma = 50$ fs) is compared with a *gedanken experiment* (black dot-dashed line) where the same density of carriers is placed *by hand* at $t = 0$ in the Γ_{15} state. With the shorter pulse, the difference between the fast $L_1 \rightarrow L'_1$ scattering and the slower $L_1 \rightarrow X_1$ transitions becomes evident.

This symmetry breaking mechanism is made possible by the external field ($V_{\mathbf{k}}$ operator in Eq. (110)) which, in the 2PPE experiment, is polarized along the crystallographic [111] direction. This breaks the $L \leftrightarrow L'$ symmetry as the operation that moves L in L' , although being a symmetry of the unperturbed system, does not leave the [111] direction unchanged. In practice this means that Eq.110 does not respect this symmetry anymore and \mathbf{k} -points connected by a rotation that does not leave the pumping field unchanged are populated in a different way. Electrons are injected in the conduction band along the $\Gamma - L$ line but not, for symmetry reasons, along the $\Gamma - L'$ line. This is clearly shown in Fig.12(a) where the population of the L'_1 state is represented with a dashed line. The L'_1 state is gradually filled while L_1 is depleted revealing that the real

source of the ultra-fast decay observed experimentally is the $L_1 \rightarrow L'_1$ scattering.

The case of bulk Silicon, as introduced in Section 2.2, well represent a key aspect of the time-resolved experiments, like TR-ARPES: the excitation process can induce processes that are not present in the equilibrium, fully interacting system, but that are induced by the driving field. Thus it is not possible to say that, in general, the time-resolved experiments simply monitor real-time, the evolution of a naturally excited system.

6.3.2. Photocarrier-induced band-gap renormalization and ultrafast charge dynamics in black phosphorus

Black phosphorus (BP) is a layered puckered structure of P atoms with remarkable anisotropic optical[202], electrical[203] and thermal properties[204]. In contrast to other layered semiconductors, the band gap in BP can be adjusted from 0.33 to 2.0 eV depending on the number of layers[205].

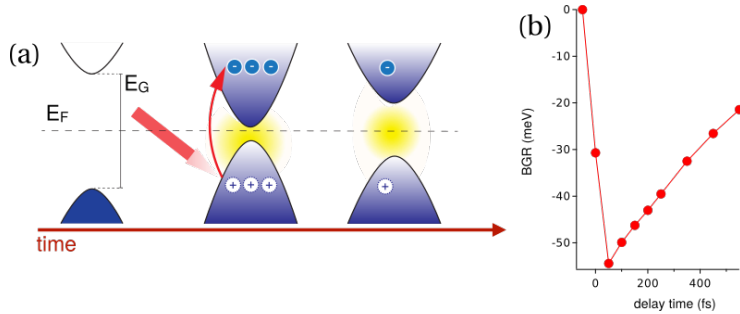


Figure 13: (a) Schematics of the BGR mechanism. Before optical excitation the Fermi level (E_F) lies within the band-gap and the valence band is fully occupied (left panel). Upon optical excitation electrons are photoexcited in the conduction band and high-energy holes are left in the valence. These high-mobility charges are responsible for the band-gap reduction (central panel). The equilibrium band-gap energy is recovered in time (right panel). (b) Simulated evolution of the BGR as a function of time. The maximum is reached slightly later than the maximum of the pump pulse.

BP is a direct gap semiconductor characterized by a wide lowest conduction band, with a large concavity that, together with the additional valleys induced by the complex electronic structure of the material dictates most of its dynamical properties.

Indeed, the response of BP to the external optical excitation is more complex than

just a variation of the occupancy of the valence and conduction states. Namely, in Ref.[193] it has been observed a sudden change in the energy position of the valence band, following the arrival of the pump pulse. The simulations performed using the *Yambo* [154, 155] code have attributed this energy shift to an ultrafast band-gap renormalization (BGR), as schematically illustrated in Fig.13(a). The band-gap shrinks (central panel), and then relaxes back to equilibrium on a longer timescale (right panel).

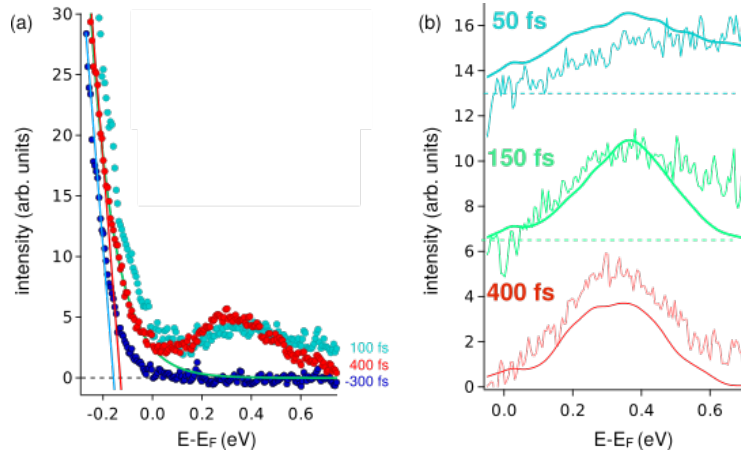


Figure 14: Quantitative comparison of the experimental and theoretical energy distribution curves (EDCs) measured at the $\bar{\Gamma}$ point. From Ref.[193]. In frame (a) the experimental EDCs are showed together with the valence band tail. In the frame (b) the experimental EDC (thin line) is compared with the simulations (thick line). The agreement is excellent.

Fig.14 presents a quantitative comparison of the experimental and theoretical BGR. Fig.14a shows three energy distribution curves (EDCs) measured at the $\bar{\Gamma}$ point. A large increase in the spectral intensity within the original gap region is observed 100 fs after the arrival of the pump. Fig.14(b) compares experimental EDCs at the $\bar{\Gamma}$ point for three delay times [50 fs (teal), 150 fs (green) and 400 fs (red)], with theoretical calculations (thin lines). The experimental data are plotted after subtracting an exponential function that fits the tail of the VB spectral intensity, as shown by the green line in Fig.14(a) for the 400 fs EDC. The excitation of hot electrons at high energy in the CB is clearly visible at 50 fs, as a broad and structureless distribution. The simulations show that the deep CB valley around the bulk Γ point accommodates most of the directly excited

carriers.

On a longer time scale, electron–electron and electron–phonon scattering mediates the relaxation of the charges towards the CBM at the bulk Z point, where they accumulate. The remarkably good agreement between experimental and calculated line shapes at 250 fs and 400 fs indicates that the measured ARPES peak reflects the density of states of the CB. This population evolves at larger delay times due to electron-hole recombination with the VB. Additional experimental and theoretical details on the excitation and the following cascade process are provided in the Supporting information.

7. Conclusion and perspectives

P&p experiments are nowadays performed on a wide family of materials that go from bulk solids to nanostructures, passing by atoms and molecules. At the same time the theoretical approaches are based on different methods and approximations. The scenario that emerges is of an exciting new field where still there is room for many years of inspiring research.

Already in the equilibrium regime the scientific community has witnessed the gradual merging of Many–Body techniques with Material Science methods. This process led to the birth of the *ab-initio* methods, which applies the well–known diagrammatic concepts in the Density–Functional Theory representation from which it takes accuracy and predictivity.

What is happening now is the gradual merging of Density–Functional Theory with Non–Equilibrium Many–Body techniques. As discussed in this review, however, there are some key differences with the equilibrium case, where there exists a well established and tested approach: the *GW/BSE*, reviewed in several works and routinely applied as coded in several public scientific codes.

In the Non–Equilibrium Many–Body approach, at the moment, there are very few scientific codes available that, in addition, use different approaches whose accuracy is still not totally assessed. Indeed the test&validate process that has been used to establish the accuracy of the *GW/BSE* approach requires many years and a large community of users. At the same time also the very basic physical processes that are triggered by the

driving pump field are still the subject of an intense debate.

The excitonic concept is a striking example of the current state-of-the-art. Considering the linear-response regime, where a tiny fraction of carriers are excited in the empty states, physical intuition would suggest that the photo-excited electrons and holes would bound together in an excitonic state. Is this what really the Non-Equilibrium Many-Body approach predicts to happen? And in case this is the right physics how can be experimentally observed? Moreover, what happens when the realistic material is considered with all relaxation processes considered?

At the moment we do not have a definitive answer to this question. But currently there is a very active research in the field that can count on the unprecedented collaboration of theory, models and *ab-initio* methods and codes, like the *Yambo* code. In addition we are gradually creating bridges with the experiments in order to unambiguously interpret the measured quantities, like the TR-ARPES, in terms of microscopic processes.

In the future we plan to continue interacting with experiments in order to assess the numerical tools based on the Non-Equilibrium Many-Body technique. We are also working to derive new theoretical schemes to be implemented in the *Yambo* code after being tested on simple models. The scenario clearly points to the need of an unprecedented collaboration of experimentalists, theoreticians and material scientists to create an universal set of public tools to be used in the scientific community providing an accurate guide for the interpretation of time-resolved experiments, like the TR-ARPES.

8. Acknowledgments

A.M. acknowledges the funding received from the European Union projects: MaX *Materials design at the eXascale* H2020-EINFRA-2015-1, Grant agreement n. 676598, and H2020-INFRAEDI-2018-2020/H2020-INFRAEDI-2018-1, Grant agreement n. 824143; *Nanoscience Foundries and Fine Analysis - Europe* H2020-INFRAIA-2014-2015, Grant agreement n. 654360. G.S. and E.P. acknowledge the financial support from MIUR PRIN (Grant No. 20173B72NB), from INFN through the TIME2QUEST project, and from Tor Vergata University through the Beyond Borders Project ULEXIEX.

Bibliography

References

- [1] K. Giesen, F. Hage, F. J. Himpsel, H. J. Riess, and W. Steinmann. Two-photon photoemission via image-potential states. *Phys. Rev. Lett.*, 55:300–303, Jul 1985.
- [2] THOMAS FAUSTER and WULF STEINMANN. Chapter 8 - two-photon photoemission spectroscopy of image states. In P. HALEVI, editor, *Photonic Probes of Surfaces*, Electromagnetic Waves: Recent Developments in Research, pages 347–411. Elsevier, Amsterdam, 1995.
- [3] P.M. Echenique, R. Berndt, E.V. Chulkov, Th. Fauster, A. Goldmann, and U. Höfer. Decay of electronic excitations at metal surfaces. *Surface Science Reports*, 52(7):219–317, 2004.
- [4] Daniele Varsano, M.A.L. Marques, and Angel Rubio. Time and energy-resolved two photon photoemission of the cu(100) and cu(111) metal surfaces. *Computational Materials Science*, 30(1):110–115, 2004. Selected papers of the Twelfth International Workshop on Computational Materials Science (CMS2002).
- [5] Xuefeng Cui, Cong Wang, Adam Argondizzo, Sean Garrett-Roe, Branko Gumhalter, and Hrvoje Petek. Transient excitons at metal surfaces. *Nature Physics*, 10(7):505–509, Jul 2014.
- [6] V. M. Silkin, P. Lazić, N. Došlić, H. Petek, and B. Gumhalter. Ultrafast electronic response of ag(111) and cu(111) surfaces: From early excitonic transients to saturated image potential. *Phys. Rev. B*, 92:155405, Oct 2015.
- [7] W. S. Fann, R. Storz, H. W. K. Tom, and J. Bokor. Electron thermalization in gold. *Phys. Rev. B*, 46:13592–13595, Nov 1992.
- [8] H. Petek and S. Ogawa. Femtosecond time-resolved two-photon photoemission studies of electron dynamics in metals. *Progress in Surface Science*, 56(4):239–310, 1997.

- [9] C. A. Schmuttenmaer, M. Aeschlimann, H. E. Elsayed-Ali, R. J. D. Miller, D. A. Mantell, J. Cao, and Y. Gao. Time-resolved two-photon photoemission from cu(100): Energy dependence of electron relaxation. *Phys. Rev. B*, 50:8957–8960, Sep 1994.
- [10] M. Lisowski, P. A. Loukakos, U. Bovensiepen, J. Stähler, C. Gahl, and M. Wolf. Ultra-fast dynamics of electron thermalization, cooling and transport effects in ru(001). *Applied Physics A*, 78(2):165–176, Jan 2004.
- [11] Martin Weinelt, Michael Kutschera, Thomas Fauster, and Michael Rohlfing. Dynamics of exciton formation at the si(100) $c(4 \times 2)$ surface. *Phys. Rev. Lett.*, 92:126801, Mar 2004.
- [12] Takeshi Suzuki and Ryo Shimano. Time-resolved formation of excitons and electron-hole droplets in si studied using terahertz spectroscopy. *Phys. Rev. Lett.*, 103:057401, Jul 2009.
- [13] Zhaogang Nie, Run Long, Linfeng Sun, Chung-Che Huang, Jun Zhang, Qihua Xiong, Daniel W. Hewak, Zexiang Shen, Oleg V. Prezhdo, and Zhi-Heng Loh. Ultrafast carrier thermalization and cooling dynamics in few-layer mos₂. *ACS Nano*, 8(10):10931–10940, 2014.
- [14] Haining Wang, Changjian Zhang, and Farhan Rana. Ultrafast dynamics of defect-assisted electron-hole recombination in monolayer mos₂. *Nano Letters*, 15(1):339–345, 2015.
- [15] J. Reimann, J. Güdde, K. Kuroda, E. V. Chulkov, and U. Höfer. Spectroscopy and dynamics of unoccupied electronic states of the topological insulators sb₂te₃ and sb₂te₂S. *Phys. Rev. B*, 90:081106, Aug 2014.
- [16] J. G. Analytis Y. L. Chen I. R. Fisher P. S. Kirchmann J. A. Sobota, S. Yang and Z.-X. Shen. *Phys. Rev. Lett.*, 108, 2012.
- [17] E. J. Sie H. Steinberg D. R. Gardner Y. S. Lee P. Jarillo-Herrero Y. H. Wang, D. Hsieh and N. Gedik. *Phys. Rev. Lett.*, 109, 2012.

- [18] F. Cilento M. Zacchigna C. Grazioli H. Berger Ph. Bugnon K. Kern M. Grioni A. Crepaldi, B. Ressel and F. Parmigiani. *Phys. Rev. B*, 86, 2012.
- [19] V. Hermann Th. Fauster T. V. Menshchikova S. V. Ereemeev Z. S. Aliev I. R. Amiraslanov M. B. Babanly P. M. Echenique D. Niesner, S. Otto and E. V. Chulkov. *Phys. Rev. B*, 89, 2014.
- [20] J. Lischner J. B. Neaton M. Bernardi, D. Vigil-Fowler and S. G. Louie. *Phys. Rev. Lett.*, 112, 2014.
- [21] N.-H. Ge, C. M. Wong, R. L. Lingle, J. D. McNeill, K. J. Gaffney, and C. B. Harris. Femtosecond dynamics of electron localization at interfaces. *Science*, 279(5348):202–205, 1998.
- [22] T. Vondrak and X.-Y. Zhu. Two-photon photoemission study of heterogeneous electron transfer: c6f6 on cu(111). *The Journal of Physical Chemistry B*, 103(17):3449–3456, 1999.
- [23] Matthias Muntwiler, Qingxin Yang, William A. Tisdale, and X.-Y. Zhu. Coulomb barrier for charge separation at an organic semiconductor interface. *Phys. Rev. Lett.*, 101:196403, Nov 2008.
- [24] X.-Y. Zhu, Q. Yang, and M. Muntwiler. Charge-transfer excitons at organic semiconductor surfaces and interfaces. *Accounts of Chemical Research*, 42(11):1779–1787, 2009.
- [25] Erwan Varene, Isabel Martin, and Petra Tegeder. Optically induced inter- and intrafacial electron transfer probed by two-photon photoemission: Electronic states of sexithiophene on au(111). *The Journal of Physical Chemistry Letters*, 2(3):252–256, 2011.
- [26] Thomas Hannappel, Bernd Burfeindt, Winfried Storck, and Frank Willig. Measurement of ultrafast photoinduced electron transfer from chemically anchored ru-dye molecules into empty electronic states in a colloidal anatase tio2 film. *The Journal of Physical Chemistry B*, 101(35):6799–6802, 1997.

- [27] Joachim Schnadt, Paul A. Brühwiler, Luc Patthey, James N. O’Shea, Sven Södergren, Michael Odelius, Rajeev Ahuja, Olof Karis, Margit Bäessler, Petter Persson, Hans Siegbahn, S. Lunell, and Nils Martensson. Experimental evidence for sub-3-fs charge transfer from an aromatic adsorbate to a semiconductor. *Nature*, 418(6898):620–623, Aug 2002.
- [28] Q Zhong, C Gahl, and M Wolf. Two-photon photoemission spectroscopy of pyridine adsorbed on cu(111). *Surface Science*, 496(1):21–32, 2002.
- [29] Ken Onda, Bin Li, and Hrvoje Petek. Two-photon photoemission spectroscopy of $\text{TiO}_2(110)$ surfaces modified by defects and O_2 or H_2O adsorbates. *Phys. Rev. B*, 70:045415, Jul 2004.
- [30] L. Miaja-Avila, G. Saathoff, S. Mathias, J. Yin, C. La-o vorakiat, M. Bauer, M. Aeschlimann, M. M. Murnane, and H. C. Kapteyn. Direct measurement of core-level relaxation dynamics on a surface-adsorbate system. *Phys. Rev. Lett.*, 101:046101, Jul 2008.
- [31] Tracy L. Thompson and John T. Yates. TiO_2 -based photocatalysis: Surface defects, oxygen and charge transfer. *Topics in Catalysis*, 35(3):197–210, Jul 2005.
- [32] David M. Adams, Louis Brus, Christopher E. D. Chidsey, Stephen Creager, Carol Creutz, Cherie R. Kagan, Prashant V. Kamat, Marya Lieberman, Stuart Lindsay, Rudolph A. Marcus, Robert M. Metzger, M. E. Michel-Beyerle, John R. Miller, Marshall D. Newton, Debra R. Rolison, Otto Sankey, Kirk S. Schanze, James Yardley, and Xiaoyang Zhu. Charge transfer on the nanoscale: current status. *The Journal of Physical Chemistry B*, 107(28):6668–6697, 2003.
- [33] X.-Y. Zhu. Photoemission from excitons in organic semiconductors. *Journal of Electron Spectroscopy and Related Phenomena*, 204:75–79, 2015. Organic Electronics.
- [34] V Saile, D Rieger, W Steinmann, and T Wegehaupt. Resonant two-photon photoemission from solid kr excited with synchrotron radiation and a n2-laser. *Physics Letters A*, 79(2):221–223, 1980.

- [35] E. Varene, L. Bogner, C. Bronner, and P. Tegeder. Ultrafast exciton population, relaxation, and decay dynamics in thin oligothiophene films. *Phys. Rev. Lett.*, 109:207601, Nov 2012.
- [36] J.-C. Deinert, D. Wegkamp, M. Meyer, C. Richter, M. Wolf, and J. Stähler. Ultrafast exciton formation at the ZnO(10 $\bar{1}$ 0) surface. *Phys. Rev. Lett.*, 113:057602, Jul 2014.
- [37] S. K. Sundaram and E. Mazur. *Nature Materials*, 1, 2002.
- [38] E. Reitsamer H. Haug D. Steinbach M. U. Wehner M. Wegener T. Marschner L. Bányai, D. B. Tran Thoai and W. Stolz. *Phys. Rev. Lett.*, 75, 1995.
- [39] S. Bar-Ad and D.S. Chemla. Quantum kinetics regime during and immediately after laser excitation of semiconductors. *Materials Science and Engineering: B*, 48(1):83–87, 1997.
- [40] D. Sangalli and A. Marini. *J. Phys.: Conf. Series*, 609, 2015.
- [41] M. Lindberg and S. W. Koch. *Phys. Rev. B*, 38, 1988.
- [42] M. Lindberg and S. W. Koch. *Phys. Rev. B*, 38, 1988.
- [43] G. Khitrova S. W. Koch, M. Kira and H. M. Gibbs. *Nature Materials*, 5, 2006.
- [44] H. Haug, , and S. W. Koch. *Quantum Theory of the Optical and Electronic Properties of Semiconductors*. World Scientific, Singapore, 1994.
- [45] A Steinhoff, M Florian, M Rösner, M Lorke, T O Wehling, C Gies, and F Jahnke. Nonequilibrium carrier dynamics in transition metal dichalcogenide semiconductors. *2D Materials*, 3(3):031006, aug 2016.
- [46] Malte Selig, Gunnar Berghäuser, Archana Raja, Philipp Nagler, Christian Schüller, Tony F. Heinz, Tobias Korn, Alexey Chernikov, Ermin Malic, and Andreas Knorr. Excitonic linewidth and coherence lifetime in monolayer transition metal dichalcogenides. *Nat Commun*, 7:026803, 2016.

- [47] Alejandro Molina-Sánchez, Davide Sangalli, Ludger Wirtz, and Andrea Marini. Ab initio calculations of ultrashort carrier dynamics in two-dimensional materials: Valley depolarization in single-layer wse₂. *Nano Letters*, 17(8):4549–4555, 2017.
- [48] Ronald Ulbricht, Euan Hendry, Jie Shan, Tony F. Heinz, and Mischa Bonn. Carrier dynamics in semiconductors studied with time-resolved terahertz spectroscopy. *Rev. Mod. Phys.*, 83:543–586, Jun 2011.
- [49] S. W. Koch, M. Kira, G. Khitrova, and H. M. Gibbs. Semiconductor excitons in new light. *Nature Materials*, 5(7):523–531, Jul 2006.
- [50] D. Sangalli E. Perfetto. A. Moarini and G. Stefanucci *Phys. Rev. B*, 94, 2016.
- [51] E. Perfetto, A. Marini, and G. Stefanucci. Self-consistent screening enhances the stability of the nonequilibrium excitonic insulator phase. *Phys. Rev. B*, 102:2791, 2020.
- [52] F. Bechstedt K. Hannewald, S. Glutsch. Theory of photoluminescence in semiconductors. *PHYSICAL REVIEW B*, 62:4519, 2000.
- [53] Gianluca Stefanucci and Robert van Leeuwen. *Nonequilibrium Many-Body Theory of Quantum Systems*. Cambridge University Press, 2013.
- [54] E. Perfetto, D. Sangalli, A. Marini, and G. Stefanucci. Nonequilibrium bethe-salpeter equation for transient photoabsorption spectroscopy. *Phys. Rev. B*, 92:205304, Nov 2015.
- [55] T. Ichibayashi and K. Tanimura. Ultrafast carrier relaxation in si studied by time-resolved two-photon photoemission spectroscopy: Intravalley scattering and energy relaxation of hot electrons. *Phys. Rev. Lett.*, 102:087403, Feb 2009.
- [56] Marco Bernardi, Derek Vigil-Fowler, Johannes Lischner, Jeffrey B. Neaton, and Steven G. Louie. Ab initio study of hot carriers in the first picosecond after sunlight absorption in silicon. *Phys. Rev. Lett.*, 112:257402, Jun 2014.

- [57] D. Sangalli and A. Marini. Ultra-fast carriers relaxation in bulk silicon following photo-excitation with a short and polarized laser pulse. *EPL (Europhysics Letters)*, 110(4):47004, 2015.
- [58] Andrea Marini. Competition between the electronic and phonon-mediated scattering channels in the out-of-equilibrium carrier dynamics of semiconductors: an ab-initio approach. *Journal of Physics: Conference Series*, 427(1):012003, 2013.
- [59] Pedro Miguel M. C. de Melo and Andrea Marini. Unified theory of quantized electrons, phonons, and photons out of equilibrium: A simplified *ab initio* approach based on the generalized baym-kadanoff ansatz. *Phys. Rev. B*, 93:155102, Apr 2016.
- [60] S.-L. Yang, J. A. Sobota, D. Leuenberger, Y. He, M. Hashimoto, D. H. Lu, H. Eisaki, P. S. Kirchmann, and Z.-X. Shen. Inequivalence of single-particle and population lifetimes in a cuprate superconductor. *Phys. Rev. Lett.*, 114:247001, Jun 2015.
- [61] A. F. Kemper, O. Abdurazakov, and J. K. Freericks. General principles for the nonequilibrium relaxation of populations in quantum materials. *Phys. Rev. X*, 8:041009, Oct 2018.
- [62] Andrea Marini, S. Ponc e, and X. Gonze. Many-body perturbation theory approach to the electron-phonon interaction with density-functional theory as a starting point. *Phys. Rev. B*, 91:224310, Jun 2015.
- [63] Feliciano Giustino. Electron-phonon interactions from first principles. *Rev. Mod. Phys.*, 89:015003, Feb 2017.
- [64] Xavier Gonze. First-principles responses of solids to atomic displacements and homogeneous electric fields: Implementation of a conjugate-gradient algorithm. *Phys. Rev. B*, 55:10337–10354, Apr 1997.

- [65] *Andrea Dal Corso Paolo Giannozzi Stefano Baroni, Stefano de Gironcoli. Phonons and related crystal properties from density-functional perturbation theory. REVIEWS OF MODERN PHYSICS, 73:515, 2001.*
- [66] *Zeng-hui Yang, Yonghui Li, and Carsten A Ullrich. A minimal model for excitons within time-dependent density-functional theory. The Journal of chemical physics, 137(1):014513, 2012.*
- [67] *G.D. Mahan. Many-Particle Physics. Plenum, 1990.*
- [68] *Henrik Bruus and Karsten Flensberg. Introduction to Many-body quantum theory in condensed matter physics. 2002.*
- [69] *A. A. Abrikosov, L. P. Gorkov, and I. E. Dzyaloshinski. Methods of quantum field theory in statistical physics. Courier Corporation, May 2012.*
- [70] *John Dirk Walecka Alexander L. Fetter. Quantum Theory of Many-particle Systems. McGraw-Hill, 1971.*
- [71] *G. Strinati. Application of the green's functions method to the study of the optical properties of semiconductors. La Rivista del Nuovo Cimento (1978-1999), 11:1–86, 1988. 10.1007/BF02725962.*
- [72] *Lars Hedin and Stig Lundqvist. Effects of electron-electron and electron-phonon interactions on the one-electron states of solids. volume 23 of Solid State Physics, pages 1 – 181. Academic Press, 1970.*
- [73] *Philip B. Allen, Marvin L. Cohen, and David R. Penn. Total dielectric function: Algebraic sign, electron-lattice response, and superconductivity. Phys. Rev. B, 38:2513–2525, Aug 1988.*
- [74] *Andrea Marini. Ab initio finite-temperature excitons. Phys. Rev. Lett., 101(10):106405, Sep 2008.*
- [75] *Giovanni Onida, Lucia Reining, and Angel Rubio. Electronic excitations: density-functional versus many-body green's-function approaches. Rev. Mod. Phys., 74(2):601–659, Jun 2002.*

- [76] *L.P. Kadanoff and G. Baym. Quantum statistical mechanics. W.A. benjamin, 1962.*
- [77] *Hartmut Haug and Antti-Pekka Jauho. Quantum kinetics in transport and optics of semiconductors. springer, 1996.*
- [78] *Robert van Leeuwen Adrian Stan, Nils Erik Dahlen. Time propagation of the kadanoff-baym equations for inhomogeneous systems. THE JOURNAL OF CHEMICAL PHYSICS, 130:224101, 2009.*
- [79] *G. Stefanucci C.-O. Almbladh R. van Leeuwen, N. E. Dahlen and U. von Barth. Lect. Notes Phys., 706, 2006.*
- [80] *P Danielewicz. Quantum theory of nonequilibrium processes, i. Annals of Physics, 152(2):239–304, 1984.*
- [81] *N. E. Dahlen and R. van Leeuwen. Phys. Rev. Lett., 98, 2007.*
- [82] *S. Bauch D. Hochstuhl, K. Balzer and M. Bonitz. Physica E, 42, 2010.*
- [83] *K. Balzer, S. Bauch, and M. Bonitz. Efficient grid-based method in nonequilibrium green's function calculations: Application to model atoms and molecules. Phys. Rev. A, 81:022510, Feb 2010.*
- [84] *K. Balzer, S. Bauch, and M. Bonitz. Time-dependent second-order born calculations for model atoms and molecules in strong laser fields. Phys. Rev. A, 82:033427, Sep 2010.*
- [85] *N.-H. Kwong and M. Bonitz. Real-time kadanoff-baym approach to plasma oscillations in a correlated electron gas. Phys. Rev. Lett., 84:1768–1771, Feb 2000.*
- [86] *D. Semkat M. Bonitz D. O. Gericke, M. S. Murillo and D. Kremp. J. Phys. A, 36, 2003.*
- [87] *M. Bonitz D. Semkat and D. Kremp. Contrib. Plasma Phys., 43, 2003.*
- [88] *M. Hartmann and W. Schäfer. Phys. Stat. Sol. (b), 173, 1992.*

- [89] D. C. Scott R. Binder W. D. Kraeft H. S. Köhler M. Bonitz, D. Kremp. J. Phys.: Cond. Matt., 8, 1996.
- [90] H. S. Köhler and R. Binder. Contrib. Plasma Phys., 37, 1997.
- [91] H. S. Köhler R. Binder and M. Bonitz. Phys. Rev. B, 55, 1997.
- [92] R. Binder N. H. Kwong, M. Bonitz and H. S. Köhler. Phys. Stat. Sol. (b), 206, 1999.
- [93] K. Balzer, M. Bonitz, R. van Leeuwen, A. Stan, and N. E. Dahlen. Nonequilibrium green's function approach to strongly correlated few-electron quantum dots. Phys. Rev. B, 79:245306, Jun 2009.
- [94] Marc Puig von Friesen, C. Verdozzi, and C.-O. Almbladh. Kadanoff-baym dynamics of hubbard clusters: Performance of many-body schemes, correlation-induced damping and multiple steady and quasi-steady states. Phys. Rev. B, 82:155108, Oct 2010.
- [95] M. Manninen N. Säkkinen and van Leeuwen R. New J. Phys., 14, 2012.
- [96] K Balzer, S Hermanns, and M Bonitz. The generalized kadanoff-baym ansatz. computing nonlinear response properties of finite systems. Journal of Physics: Conference Series, 427:012006, mar 2013.
- [97] C. Verdozzi Marc Puig von Friesen. and C.-O. Almbladh Phys. Rev. B, 82, 2010.
- [98] V. M. Turkowski J. K. Freericks and V. Zlatic. Phys. Rev. Lett., 97, 2006.
- [99] M. Kollar M. Eckstein and P. Werner. Phys. Rev. B, 81, 2010.
- [100] M. Eckstein and P. Werner. Phys. Rev. B, 82, 2010.
- [101] G. Stefanucci P. Myöhänen, A. Stan and R. van Leeuwen. Europhys. Lett., 84, 2008.
- [102] G. Stefanucci P. Myöhänen, A. Stan and R. van Leeuwen. Phys. Rev. B, 80, 2009.

- [103] *M. Puig von Friesen, C. Verdozzi, and C.-O. Almbladh. Successes and failures of kadanoff-baym dynamics in hubbard nanoclusters. Phys. Rev. Lett., 103:176404, Oct 2009.*
- [104] *G. Stefanucci P. Myöhänen, A. Stan and R. van Leeuwen. J. Phys.: Conf. Series, 220, 2010.*
- [105] *A. Alvermann T. Koch, J. Loos. and H. Fehske Phys. Rev. B, 84, 2011.*
- [106] *A. Stan G. Stefanucci S. Kurth A.-M. Uimonen, E. Khosravi. R. van Leeuwen and E. K. U. Gross Phys. Rev. B, 84, 2011.*
- [107] *A. Stan G. Stefanucci S. Kurth E. Khosravi, A.-M. Uimonen. R. van Leeuwen and E. K. U. Gross Phys. Rev. B, 85, 2012.*
- [108] *E. Perfetto and G. Stefanucci. Phys. Rev. B, 88, 2013.*
- [109] *D. Karlsson and C. Verdozzi. Phys. Rev. B, 90, 2014.*
- [110] *V. Špička P. Lipavský and B. Velický. Phys. Rev. B, 34, 1986.*
- [111] *R. van Leeuwen E. Perfetto, A.-M. Uimonen and G. Stefanucci. Phys. Rev. A, 92, 2015.*
- [112] *B. Arnaud, S. Lebègue, and M. Alouani. Excitonic and quasiparticle lifetime effects on silicon electron energy loss spectra from first principles. Phys. Rev. B, 71:035308, Jan 2005.*
- [113] *A. Marini and R. Del Sole. Phys. Rev. Lett., 91, 2003.*
- [114] *H. Haug. Phys. Status Solidi B, 173, 1992.*
- [115] *D. Semkat M. Bonitz and H. Haug. Eur. Phys. J. B, 9, 1999.*
- [116] *A. Marini. J. Phys. Conf. Ser., 427, 2013.*
- [117] *A.-M. Uimonen R. van Leeuwen S. Latini, E. Perfetto and G. Stefanucci. Phys. Rev. B, 89, 2014.*

- [118] Sebastian Hermanns, Niclas Schlünzen, and Michael Bonitz. *Hubbard nanoclusters far from equilibrium*. Phys. Rev. B, 90:125111, Sep 2014.
- [119] Niclas Schlünzen, Sebastian Hermanns, Michael Bonitz, and Claudio Verdozzi. *Dynamics of strongly correlated fermions: Ab initio results for two and three dimensions*. Physical Review B, 93(3):035107, 2016.
- [120] Yevgeny Bar Lev and David R Reichman. *Dynamics of many-body localization*. Physical Review B, 89(22):220201, 2014.
- [121] Miroslav Hopjan, Gianluca Stefanucci, Enrico Perfetto, and Claudio Verdozzi. *Molecular junctions and molecular motors: Including coulomb repulsion in electronic friction using nonequilibrium green's functions*. Physical Review B, 98(4):041405, 2018.
- [122] Riku Tuovinen, Robert van Leeuwen, Enrico Perfetto, and Gianluca Stefanucci. *Electronic transport in molecular junctions: The generalized kadanoff–baym ansatz with initial contact and correlations*. The Journal of Chemical Physics, 154(9):094104, 2021.
- [123] F. Cosco, N. W. Talarico, R. Tuovinen, and N. Lo Gullo, 2020.
- [124] Fabio Covito, Enrico Perfetto, Angel Rubio, and Gianluca Stefanucci. *Benchmarking nonequilibrium green's functions against configuration interaction for time-dependent auger decay processes*. The European Physical Journal B, 91(10):1–7, 2018.
- [125] E Perfetto, A-M Uimonen, Robert van Leeuwen, and G Stefanucci. *Time-resolved photoabsorption in finite systems: a first-principles negf approach*. In Journal of Physics: Conference Series, volume 696, page 012004. IOP Publishing, 2016.
- [126] E. Perfetto, D. Sangalli, A. Marini, and G. Stefanucci. *Ultrafast Charge Migration in XUV Photoexcited Phenylalanine: A First-Principles Study Based on Real-Time Nonequilibrium Green's Functions*. J. Phys. Chem. Lett., 9(6):1353–1358, 2018.

- [127] E. Perfetto, D. Sangalli, M. Palumbo, A. Marini, and G. Stefanucci. *First-Principles Nonequilibrium Green's Function Approach to Ultrafast Charge Migration in Glycine*. *J. Chem. Theory Comput.*, 15(8):4526–4534, 2019.
- [128] E Perfetto, A Trabattoni, F Calegari, M Nisoli, A Marini, and G Stefanucci. *Ultrafast Quantum Interference in the Charge Migration of Tryptophan*. *J. Phys. Chem. Lett.*, page 9, 2020.
- [129] Erik P Mansson, Simone Latini, Fabio Covito, Vincent Wanie, Mara Galli, Enrico Perfetto, Gianluca Stefanucci, Hannes Huebener, Umberto De Giovannini, Mattea C Castrovilli, et al. *Correlation-driven sub-3 fs charge migration in ionised adenine*. arXiv preprint arXiv:2101.05753, 2021.
- [130] Emil Viñas Boström, Anders Mikkelsen, Claudio Verdozzi, Enrico Perfetto, and Gianluca Stefanucci. *Charge Separation in Donor-C₆₀ Complexes with Real-Time Green Functions: The Importance of Nonlocal Correlations*. *Nano Lett.*, 18(2):785–792, 2018.
- [131] Yuta Murakami, Michael Schüler, Shintaro Takayoshi, and Philipp Werner. *Ultrafast nonequilibrium evolution of excitonic modes in semiconductors*. *Phys. Rev. B*, 101(3):035203, 2020.
- [132] Riku Tuovinen, Golež Denis, Michael Schüler, Philipp Werner, Martin Eckstein, and Michael A. Sentef. *Adiabatic preparation of a correlated symmetry-broken initial state with the generalized kadanoff–baym ansatz*. *physica status solidi (b)*, 0(0):1800469.
- [133] Riku Tuovinen, Denis Golez, Martin Eckstein, and Michael A. Sentef. *Comparing the generalized Kadanoff-Baym ansatz with the full Kadanoff-Baym equations for an excitonic insulator out of equilibrium*. *Phys. Rev. B*, 102(11):115157, 2020.
- [134] G. Pal, Y. Pavlyukh, W. Hübner, and H. C. Schneider. *Optical absorption spectra of finite systems from a conserving Bethe-Salpeter equation approach*. *Eur. Phys. J. B*, 79:327–334, 2011.

- [135] E. Perfetto, D. Sangalli, A. Marini, and G. Stefanucci. *Nonequilibrium bethe-salpeter equation for transient photoabsorption spectroscopy*. Phys. Rev. B, 92:205304, Nov 2015.
- [136] C. Manzoni G. Cerullo D. Sangalli, S. Dal Conte and A. Marini. Phys. Rev. B, 93, 2016.
- [137] Eva A. A. Pogna, Margherita Marsili, Domenico De Fazio, Stefano Dal Conte, Cristian Manzoni, Davide Sangalli, Duhee Yoon, Antonio Lombardo, Andrea C. Ferrari, Andrea Marini, Giulio Cerullo, and Deborah Prezzi. *Photo-induced bandgap renormalization governs the ultrafast response of single-layer mos₂*. ACS Nano, 10(1):1182–1188, 2016. PMID: 26691058.
- [138] Alejandro Molina-Sánchez, Davide Sangalli, Ludger Wirtz, and Andrea Marini. *Ab initio calculations of ultrashort carrier dynamics in two-dimensional materials: Valley depolarization in single-layer wse₂*. Nano Letters, 17(8):4549–4555, 2017. PMID: 28692278.
- [139] Niclas Schliinzen, Jan-Philip Joost, and Michael Bonitz. *Achieving the Scaling Limit for Nonequilibrium Green Functions Simulations*. Phys. Rev. Lett., 124(7):076601, 2020.
- [140] Jan-Philip Joost, Niclas Schliinzen, and Michael Bonitz. *G1-G2 scheme: Dramatic acceleration of nonequilibrium Green functions simulations within the Hartree-Fock generalized Kadanoff-Baym ansatz*. Phys. Rev. B, 101(24):245101, 2020.
- [141] Yaroslav Pavlyukh, Enrico Perfetto, and Gianluca Stefanucci. *Photoinduced dynamics of organic molecules using nonequilibrium green’s functions with second-born, gw, t-matrix and three-particle ladder correlations*. arXiv preprint arXiv:2103.11932, 2021.
- [142] J K Freericks, H R Krishnamurthy, M A Sentef, and T P Devereaux. *Gauge invariance in the theoretical description of time-resolved angle-resolved pump/probe photoemission spectroscopy*. T165:014012, oct 2015.

- [143] R. Bertoni and A. P. Jauho. *Gauge-invariant formulation of the intracollisional field effect including collisional broadening*. Phys. Rev. B, 44:3655–3664, Aug 1991.
- [144] E. Perfetto, D. Sangalli, A. Marini, and G. Stefanucci. *First-principles approach to excitons in time-resolved and angle-resolved photoemission spectra*. Physical Review B, 94(24):245303, 2016.
- [145] H. R. Krishnamurthy, J. K. Freericks, and Th. Pruschke. Phys. Rev. Lett., 102, 2009.
- [146] E. Perfetto, S. Bianchi, and G. Stefanucci. *Time-resolved arpes spectra of nonequilibrium excitonic insulators: Revealing macroscopic coherence with ultrashort pulses*. Phys. Rev. B, 101:2791, 2020.
- [147] E. Perfetto and G. Stefanucci. *Floquet topological phase of nondriven p-wave nonequilibrium excitonic insulators*. Phys. Rev. Lett., 125, 2020.
- [148] H. Tanimura, K. Tanimura, and P. H. M. van Loosdrecht. *Dynamics of incoherent exciton formation in Cu₂O: Time- and angle-resolved photoemission spectroscopy*. Phys. Rev. B, 100:115204, Sep 2019.
- [149] Julien Madéo, Michael K. L. Man, Chakradhar Sahoo, Marshall Campbell, Vivek Pareek, E. Laine Wong, Abdullah Al-Mahboob, Nicholas S. Chan, Arka Karmakar, Bala Murali Krishna Mariserla, Xiaoqin Li, Tony F. Heinz, Ting Cao, and Keshav M. Dani. *Directly visualizing the momentum-forbidden dark excitons and their dynamics in atomically thin semiconductors*. Science, 370:1199–1204, 2020.
- [150] Avinash Rustagi and Alexander F. Kemper. *Photoemission signature of excitons*. Phys. Rev. B, 97, 2018.
- [151] Robert Wallauer, Raul Perea-Causin, Lasse Münster, Sarah Zajusch, Samuel Brem, Jens Güdde, Katsumi Tanimura, Kai-Qiang Lin, Rupert Huber, Ermin Malic, and et al. *Momentum-resolved observation of exciton formation dynamics in monolayer ws₂*. Nano Letters, 21(13):5867–5873, Jun 2021.

- [152] Alexander F. Kemper and Avinash Rustagi. *Observing coherences with time-resolved photoemission*, 2020.
- [153] Keisuke Fukutani, Roland Stania, Chang Il Kwon, Jun Sung Kim, Ki Jeong Kong, Jaeyoung Kim, and Han Woong Yeom. *Detecting photoelectrons from spontaneously formed excitons*, 2021.
- [154] Davide Sangalli, Andrea Ferretti, Henrique Miranda, Claudio Attaccalite, Ivan Marri, Elena Cannuccia, Pedro Miguel Melo, Margherita Marsili, Fulvio Paleari, Antimo Marrazzo, Gianluca Prandini, Pietro Bonfà, Michael O Atambo, Fabio Affinito, Maurizia Palumbo, Alejandro Molina Sanchez, Conor Hogan, Myrta Grüning, Daniele Varsano, and Andrea Marini. *Many-body perturbation theory calculations using the yambo code*. *Journal of Physics: Condensed Matter*, 31:325902, 2019.
- [155] Myrta Grüning Daniele Varsano Andrea Marini, Conor Hogan. *yambo: An ab initio tool for excited state calculations*. *Computer Physics Communications*, 180:1392–1403, 2009.
- [156] Pierluigi Cudazzo. *First-principles description of the exciton-phonon interaction: A cumulant approach*. *Phys. Rev. B*, 102:449, 2020.
- [157] Galan Moody, Chandriker Kavir Dass, Kai Hao, Chang-Hsiao Chen, Lain-Jong Li, Akshay Singh, Kha Tran, Genevieve Clark, Xiaodong Xu, Gunnar Berghäuser, Ermin Malic, Andreas Knorr, and Xiaoqin Li. *Intrinsic homogeneous linewidth and broadening mechanisms of excitons in monolayer transition metal dichalcogenides*. *Nat Commun*, 6:136805, 2015.
- [158] S. Shree, M. Semina, C. Robert, B. Han, T. Amand, A. Balocchi, M. Manca, E. Courtade, X. Marie, T. Taniguchi, K. Watanabe, M. M. Glazov, and B. Urbaszek. *Observation of exciton-phonon coupling in MoSe_2 monolayers*. *Phys. Rev. B*, 98, 2018.
- [159] A. O. Slobodeniuk and D. M. Basko. *Exciton-phonon relaxation bottleneck and*

- radiative decay of thermal exciton reservoir in two-dimensional materials.* Phys. Rev. B, 94:223, 2016.
- [160] Hsiao-Yi Chen, Davide Sangalli, and Marco Bernardi. *Exciton-phonon interaction and relaxation times from first principles.* Phys. Rev. Lett., 125, 2020.
- [161] Florian Katsch, Malte Selig, Alexander Carmele, and Andreas Knorr. *Theory of exciton–exciton interactions in monolayer transition metal dichalcogenides.* Phys. Status Solidi B, 255:1800185, 2018.
- [162] Monique Combescot, Roland Combescot, and François Dubin. *Bose–einstein condensation and indirect excitons: a review.* Rep. Prog. Phys., 80:066501, 2017.
- [163] S. A. Moskalenko and D. W. Snoke. *Bose-Einstein Condensation of Excitons and Biexcitons: And Coherent Nonlinear Optics with Excitons.* Cambridge University Press, 2000.
- [164] S. Schmitt-Rink, D. S. Chemla, and H. Haug. *Nonequilibrium theory of the optical stark effect and spectral hole burning in semiconductors.* Phys. Rev. B, 37:941–955, Jan 1988.
- [165] S. Glutsch, F. Bechstedt, and R. Zimmermann. *Optical excitation and bose condensation of excitons in low-dimensional systems.* physica status solidi (b), 172(1):357–369, 1992.
- [166] K Hannewald, S Glutsch, and F Bechstedt. *Excitonic insulator through coherent pulse excitation?* Journal of Physics: Condensed Matter, 13(2):275–286, dec 2000.
- [167] Dominik Christiansen, Malte Selig, Ermin Malic, Ralph Ernstorfer, and Andreas Knorr. *Theory of exciton dynamics in time-resolved arpes: Intra- and intervalley scattering in two-dimensional semiconductors.* Phys. Rev. B, 100:18, 2019.
- [168] E. Perfetto, D. Sangalli, A. Marini, and G. Stefanucci. *Pump-driven normal-to-excitonic insulator transition: Josephson oscillations and signatures of bec-bcs crossover in time-resolved arpes.* Phys. Rev. Materials, 3:2791, 2019.

- [169] *Maciej Dendzik, R. Patrick Xian, Enrico Perfetto, Davide Sangalli, Dmytro Kutnyakhov, Shuo Dong, Samuel Beaulieu, Tommaso Pincelli, Federico Pressacco, Davide Curcio, Steinn Ymir Agustsson, Michael Heber, Jasper Hauer, Wilfried Wurth, Günter Brenner, Yves Acremann, Philip Hofmann, Martin Wolf, Andrea Marini, Gianluca Stefanucci, Laurenz Rettig, and Ralph Ernstorfer. Observation of an excitonic mott transition through ultrafast core-cum-conduction photoemission spectroscopy. Phys. Rev. Lett., 125, 2020.*
- [170] *E Perfetto and G Stefanucci. Ultrafast creation and melting of nonequilibrium excitonic condensates in bulk wse $_2$. arXiv preprint arXiv:2011.11967, 2020.*
- [171] *Th. Östreich and K. Schönhammer. Non-stationary excitonic-insulator states in photoexcited semiconductors. Zeitschrift für Physik B Condensed Matter, 91(2):189–197, Jun 1993.*
- [172] *M Yamaguchi, K Kamide, T Ogawa, and Y Yamamoto. BEC–BCS-laser crossover in coulomb-correlated electron–hole–photon systems. New Journal of Physics, 14(6):065001, jun 2012.*
- [173] *Makoto Yamaguchi, Kenji Kamide, Ryota Nii, Tetsuo Ogawa, and Yoshihisa Yamamoto. Second thresholds in bec-bcs-laser crossover of exciton-polariton systems. Phys. Rev. Lett., 111:026404, Jul 2013.*
- [174] *R. Hanai, P. B. Littlewood, and Y. Ohashi. Non-equilibrium properties of a pumped-decaying bose-condensed electron–hole gas in the bcs–bec crossover region. Journal of Low Temperature Physics, 183(3):127–135, May 2016.*
- [175] *Ryo Hanai, Peter B. Littlewood, and Yoji Ohashi. Dynamical instability of a driven-dissipative electron-hole condensate in the bcs-bec crossover region. Phys. Rev. B, 96:125206, Sep 2017.*
- [176] *Christopher Triola, Anna Pertsova, Robert S. Markiewicz, and Alexander V. Balatsky. Excitonic gap formation in pumped dirac materials. Phys. Rev. B, 95:205410, May 2017.*

- [177] Ryo Hanai, Peter B. Littlewood, and Yoji Ohashi. *Photoluminescence and gain/absorption spectra of a driven-dissipative electron-hole-photon condensate*. Phys. Rev. B, 97:245302, Jun 2018.
- [178] Anna Pertsova and Alexander V. Balatsky. *Excitonic instability in optically pumped three-dimensional dirac materials*. Phys. Rev. B, 97:075109, Feb 2018.
- [179] Klaus W. Becker, Holger Fehske, and Van-Nham Phan. *Projector-based renormalization approach to electron-hole-photon systems in their nonequilibrium steady state*. Phys. Rev. B, 99:035304, Jan 2019.
- [180] Yuta Murakami, Michael Schüler, Shintaro Takayoshi, and Philipp Werner. *Ultrafast nonequilibrium evolution of excitonic modes in semiconductors*. Phys. Rev. B, 101:197, 2020.
- [181] M. H. Szymańska, J. Keeling, and P. B. Littlewood. *Nonequilibrium quantum condensation in an incoherently pumped dissipative system*. Phys. Rev. Lett., 96:230602, Jun 2006.
- [182] Michael KL Man, Julien Madéo, Chakradhar Sahoo, Kaichen Xie, Marshall Campbell, Vivek Pareek, Arka Karmakar, E Laine Wong, Abdullah Al-Mahboob, Nicholas S Chan, et al. *Experimental measurement of the intrinsic excitonic wavefunction*. arXiv preprint arXiv:2011.13104, 2020.
- [183] Shuo Dong, Michele Puppini, Tommaso Pincelli, Samuel Beaulieu, Dominik Christiansen, Hannes Hubener, Christopher W Nicholson, R Patrick Xian, Maciej Dendzik, Yunpei Deng, et al. *Measurement of an excitonic wave function*. arXiv preprint arXiv:2012.15328, 2020.
- [184] Hartmut Haug and Stephan W. Koch. *Quantum theory of the optical and electronic properties of semiconductors*. World Scientific, 2004.
- [185] Alexander Steinhoff, Matthias Florian, Malte Rösner, Michael Lorke, Tim O Wehling, Christopher Gies, and Frank Jahnke. *Nonequilibrium carrier dynamics in transition metal dichalcogenide semiconductors*. 2D Materials, 3(3):031006, 2016.

- [186] Ronald Ulbricht, Euan Hendry, Jie Shan, Tony F Heinz, and Mischa Bonn. *Carrier dynamics in semiconductors studied with time-resolved terahertz spectroscopy*. *Reviews of Modern Physics*, 83(2):543, 2011.
- [187] M. Rösner M. Schönhoff G. Wehling T. O. Jahnke F. Steinhoff, A. Florian. *Exciton fission in monolayer transition metal dichalcogenide semiconductors*. *Nature Communications*, 8:1166, 2017.
- [188] Davide Sangalli and Andrea Marini. *Complete collisions approximation to the kadanoff-baym equation: a first-principles implementation*. *Journal of Physics: Conference Series*, 609(1):012006, 2015.
- [189] Davide Sangalli, Stefano Dal Conte, Cristian Manzoni, Giulio Cerullo, and Andrea Marini. *Nonequilibrium optical properties in semiconductors from first principles: A combined theoretical and experimental study of bulk silicon*. *Phys. Rev. B*, 93:195205, May 2016.
- [190] Valerie Smejkal, Florian Libisch, Alejandro Molina-Sanchez, Chiara Trovatello, Ludger Wirtz, and Andrea Marini. *Time-dependent screening explains the ultrafast excitonic signal rise in 2d semiconductors*. *ACS Nano*, 15:1179–1185, 2021.
- [191] Chiara Trovatello, Henrique P. C. Miranda, Alejandro Molina-Sánchez, Rocío Borrego-Varillas, Cristian Manzoni, Luca Moretti, Lucia Ganzer, Margherita Maiuri, Junjia Wang, Dumitru Dumcenco, Andras Kis, Ludger Wirtz, Andrea Marini, Giancarlo Soavi, Andrea C. Ferrari, Giulio Cerullo, Davide Sangalli, and Stefano Dal Conte. *Strongly coupled coherent phonons in single-layer mos_2* . *ACS Nano*, 14:5700–5710, 2020.
- [192] Zilong Wang, Alejandro Molina-Sánchez, Patrick Altmann, Davide Sangalli, Domenico De Fazio, Giancarlo Soavi, Ugo Sassi, Federico Bottegoni, Franco Ciccacci, Marco Finazzi, Ludger Wirtz, Andrea C. Ferrari, Andrea Marini, Giulio Cerullo, and Stefano Dal Conte. *Intravalley spin-flip relaxation dynamics in single-layer ws*. *Nano Lett.*, 18:6882–6891, 2018.

- [193] S Roth, A Crepaldi, M Puppini, G Gatti, D Bugini, I Grimaldi, T R Barrilot, C A Arrell, F Frassetto, L Poletto, M Chergui, A Marini, and M Grioni. *Photocarrier-induced band-gap renormalization and ultrafast charge dynamics in black phosphorus*. *2D Mater.*, 6:031001, 2019.
- [194] M. Grüning C. Attaccalite and A. Marini. *Real-time approach to the optical properties of solids and nanostructures: Time-dependent bethe-salpeter equation*. *Phys. Rev. B*, 84:245110, Dec 2011.
- [195] Stefan Albrecht, Lucia Reining, Rodolfo Del Sole, and Giovanni Onida. *Ab initio calculation of excitonic effects in the optical spectra of semiconductors*. *Phys. Rev. Lett.*, 80(20):4510–4513, May 1998.
- [196] Martin Schultze, Krupa Ramasesha, C.D. Pemmaraju, S.A. Sato, D. Whitmore, A. Gandman, James S. Prell, L. J. Borja, D. Prendergast, K. Yabana, Daniel M. Neumark, and Stephen R. Leone. *Attosecond band-gap dynamics in silicon*. *Science*, 346(6215):1348–1352, 2014.
- [197] Ryo Shimano and Takeshi Suzuki. *Exciton mott transition in si studied by terahertz spectroscopy*. *physica status solidi (c)*, 8(4):1153–1156, 2011.
- [198] Takeshi Suzuki and Ryo Shimano. *Time-resolved formation of excitons and electron-hole droplets in si studied using terahertz spectroscopy*. *Phys. Rev. Lett.*, 103(5):057401, Jul 2009.
- [199] Valerio Olevano and Lucia Reining. *Excitonic effects on the silicon plasmon resonance*. *Phys. Rev. Lett.*, 86:5962–5965, Jun 2001.
- [200] Masayuki Constantinescu Anca Monia Petek Hrvoje Hase, Muneaki Katsuragawa. *Frequency comb generation at terahertz frequencies by coherent phonon excitation in silicon*. *Nat Photon*, 6:243, 2012/04/print.
- [201] Masahiro Constantinescu Anca Monia Petek Hrvoje Hase, Muneaki Kitajima. *The birth of a quasiparticle in silicon observed in time-frequency space*. *Nature*, 426:51, 2003/11/06/print.

- [202] X. Wang, A. M. Jones, K. L. Seyler, V. Tran, Y. Jia, H. Zhao, H. Wang, L. Yang, X. Xu, and F. Xia. *Highly anisotropic and robust excitons in monolayer black phosphorus*. *Nat. Nanotech.*, 10(6):517–521, 2015.
- [203] F. Xia, H. Wang, and Y. Jia. *Rediscovering black phosphorus as an anisotropic layered material for optoelectronics and electronics*. *Nat. Commun.*, 5:4458, 2015.
- [204] Z. Luo, J. Maassen, Y. Deng, Y. Du, R. P. Garrelts, M. S. Lundstrom, P. D. Ye, and X. Xu. *Anisotropic in-plane thermal conductivity observed in few-layer black phosphorus*. *Nat. Commun.*, 6:8572, 2015.
- [205] Vy Tran, Ryan Soklaski, Yufeng Liang, and Li Yang. *Layer-controlled band gap and anisotropic excitons in few-layer black phosphorus*. *Phys. Rev. B*, 89:235319, Jun 2014.